Received: 2 December 2022 | Revised: 15 February 2023 | Accepted: 20 February 2023

DOI: 10.1002/esp.5569

RESEARCH ARTICLE

ESPL WILEY

Active temperate glacial landsystem evolution in association with outwash head/depositional overdeepenings

David J. A. Evans[1] | Marek W. Ewertowski[2] | Aleksandra Tomczyk[2] | Benjamin M. P. Chandler[3]

[1]Department of Geography, Durham University, Durham, UK

[2]Faculty of Geographical and Geological Sciences, Adam Mickiewicz University, Poznań, Poland

[3]School of Geography, University of Nottingham, Nottingham, UK

Correspondence
David J. A. Evans, Department of Geography, Durham University, South Road, Durham DH1 3LE, UK.
Email: d.j.a.evans@durham.ac.uk

Funding information
Narodowe Centrum Nauki, Grant/Award Number: 2019/35/B/ST10/03928

Abstract

The response of temperate glaciers to rapid climate warming is reflected in the geomorphology (landsystem) resulting from snout recession. This paper develops a locally diverse process-form model of active temperate glaciers through mapping and quantification of historical landscape change on the Fjallsjökull-Hrútárjökull foreland, SE Iceland. Quantification of volumetric and areal changes on the foreland are based on time series of archival aerial images for the period 1945–1998, high-resolution satellite imagery for 2014 and digital elevation models of differences derived from time series of UAV imagery for the years 2014, 2016, 2018, 2019 and 2022. Landscape change and glacier snout behaviour since 1945 highlights the importance of azonal and potentially intrazonal signatures in temperate glacial landsystems, particularly: (1) the development and collapse of partially supraglacial outwash fans to produce outwash heads fronting depositional overdeepenings; and (2) the emergence of ice-cored eskers that record the evolution of englacial drainage networks operating over overdeepenings. Such landform assemblages are manifested as substantial ice-cored/hummocky terrains, a characteristic of deglaciating forelands that is likely to be widely replicated wherever ice-contact glacifluvial assemblages create outwash heads that act as depositional overdeepenings. Due to its significantly greater supraglacial debris cover, complete de-icing of the Hrútárjökull snout in response to post-1945 warming was delayed until around 2014. This constitutes a prime example of incremental stagnation, which in a rapidly warming climate has resulted in significant landscape change (land surface elevation collapse of 0.8 m a^{-1}) over the last 8 years.

KEYWORDS
depositional overdeepening, Fjallsjökull-Hrútárjökull, glacial process-form regimes, Iceland, landscape change quantification, outwash head

1 | INTRODUCTION

Assessments of the spatial and temporal evolution of modern glacial landsystems are invaluable analogues in efforts to reconstruct glacier-climate interactions from geomorphological signatures in ancient deglaciated terrains (e.g. Benn & Evans, 2010; Evans, 2003, 2013 and references cited therein). Icelandic glaciers have been widely utilized in this way (e.g. Bennett & Evans, 2012; Evans, 2005, 2009; Evans & Twigg, 2002; Evans et al., 1999; Eyles, 1983; Kjær & Krüger, 2001; Krüger, 1994; Maizels, 1997; Price, 1969; Russell et al., 2006; Schomacker et al., 2009; Thórarinsson, 1939, 1943), especially those of the south coast, where post-Little Ice Age (LIA) recession is well documented both in historical archives and aerial imagery. This has facilitated the linkage of short-timescale glacial process-form regimes to climate trends at relatively high resolution (e.g. Boulton, 1986; Bradwell et al., 2013; Chandler et al., 2016a, 2016b, 2016; Chandler, Chandler, et al., 2020; Chandler, Evans, et al., 2020; Evans & Twigg, 2002; Evans et al., 2016, 2017a, 2017b, 2018; Evans,

Ewertowski, et al., 2019; Evans, Guðmundsson, et al., 2019). The local overprinting and/or switching of predominantly active temperate glacial landsystem signatures (classified as azonal and intrazonal changes by Evans, 2013) is especially important. With the exception of the intermittent surge activity documented at Skeiðarárjökull and Breiðamerkurjökull (Björnsson et al., 2003; Evans & Twigg, 2002; Russell et al., 2001; Waller et al., 2008), these azonal/intrazonal changes are triggered by either significant climate changes (e.g. Bradwell et al., 2013; Chandler, Evans, et al., 2020; Evans et al., 2017a) and/or topographically controlled changes to the morphology and structure of receding glacier snouts (e.g. Evans, Ewertowski, et al., 2019; Phillips et al., 2013).

Spatial and temporal changes in the landsystem signatures of some glacier snouts in southern Iceland are trending towards a set of process-form regimes indicative of the accelerated climate warming of the late 20th to early 21st centuries. This involves an apparent switch from annual push moraine formation typical of active temperate glaciers to downwasting and calving in expanding proglacial lakes (Bennett & Evans, 2012; Bennett et al., 2010; Phillips et al., 2013). However, these changes are not wholly climate-driven, as they have also been conditioned by snout recession into overdeepenings. In southeast Iceland, retreating piedmont lobes are rapidly uncovering depositional overdeepenings, or depressions formed inside the former ice-contact slopes of sandur fans (outwash heads; sensu Benn et al., 2003; Kirkbride, 2000), which may coincide with erosional overdeepenings (e.g. Bennett & Evans, 2012; Spedding & Evans, 2002). In some locations these depressions, especially where they are associated with erosional overdeepenings (e.g. Kviárjökull, Heinabergsjökull and Hoffellsjokull; Bennett & Evans, 2012; Evans & Orton, 2015; Evans, Ewertowski, et al., 2019), are large enough to switch whole snouts into floating and calving mode. However, this may not constitute intrazonal landsystem change but rather azonal change, whereby local topographic conditions switch the process-form regime temporarily.

Such switching of process-form regimes is well demonstrated on the foreland of Fjallsjökull, where rapid calving into proglacial lake Fjallsarlón presently characterizes the northern part of the glacier snout (Dell et al., 2019). In contrast, on the south foreland, depositional overdeepenings have been evolving in the former coalescence zone of Fjallsjökull and Hrútárjökull since around 1945 (Chandler, Chandler, et al., 2020; Evans et al., 2009; Guðmundsson et al., 2019). During the production of these overdeepenings and their associated landform–sediment assemblages, the glacier margins have continued in active temperate mode (Chandler et al., 2016a, 2016b; Evans et al., 2009), with the snout of Hrútárjökull also developing a significant supraglacial debris cover on its right lateral margin. The localized influence of depositional overdeepenings on the Fjallsjökull-Hrútárjökull foreland has provided an azonal landsystem signature on a historical and therefore measurable timescale. The aim of this study was to map these emerging glacial landsystem signatures to quantify landscape change on the Fjallsjökull-Hrútárjökull foreland, enabling the development of locally diverse process-form models that reflect the response of individual temperate glaciers to rapid climate warming. Specifically, it provides a detailed analysis of the complex assemblage of ice-cored landforms that have emerged during glacier snout downwasting and recession inside outwash heads (depositional overdeepenings) in the former coalescence zone of Fjallsjökull and Hrútárjökull.

2 | FJALLSJÖKULL-HRÚTÁRJÖKULL: STUDY AREA AND PREVIOUS RESEARCH

The piedmont lobes of Fjallsjökull and Hrútárjökull are two of many that are nourished by ice flowing out from the Öræfi caldera (Figure 1). Formerly coalescent until ~2010 (Hannesdóttir et al., 2015), they descend rapidly from their accumulation zone at ~1000 m to near sea level over a distance of ca. 6 km. These outlet glaciers flow over a series of bedrock steps to form some of the most spectacular ice falls in Iceland (Figure 1). While the dimensions of the erosional overdeepenings beneath Fjallsjökull and Hrútárjökull have been reported (Magnusson et al., 2012) and their influence on ice margin recession evaluated (Hannesdóttir et al., 2014, 2015; Figure 1b), no analysis has been undertaken on the emergence and development of the depositional overdeepenings in the area of downwasting and decoupling of the two snouts to the south (Figures 1 and 2).

The geomorphology of this area of the foreland has been represented by Chandler, Chandler, et al. (2020) in their map based upon imagery for the year 2012 (Figure 3). This depicts an area mapped as overdeepening deposits (on the south Fjallsjökull margin) and ice-cored hummocky terrain (along the Hrútárjökull margin), together with small areas of kame and kettle topography, which are increasingly common landform–sediment associations in recently deglaciated forelands in southern Iceland (e.g. Bennett & Evans, 2012; Bennett et al., 2010; Chandler, Chandler, et al., 2020; Evans et al., 2017a, 2017b, 2018, 2009). The sediment assemblages in such areas are related not only to supraglacial moraine construction but also to the widespread development of complex ice-contact glacifluvial processes, whereby englacial esker networks feeding into ice-marginal and proglacial outwash (sandur) fans progressively enlarge and bury downwasting snouts. This results in a hummocky kame and kettle topography that, since the benchmark process-form studies of Price (1969, 1971, 1973) and Howarth (1971), has been acknowledged as the product of widespread de-icing/melt-out of buried glacier ice (e.g. Chandler, Chandler, et al., 2020; Evans & Orton, 2015; Evans & Twigg, 2002; Evans et al., 2009, 2018; Storrar et al., 2015). An appreciation of the greater importance of glacifluvial rather than supraglacial topographic reversal origins of such hummocky terrain on deglaciating Icelandic forelands has alerted glacial geomorphologists to the limitations on, and localized nature of, supraglacial hummocky moraine generation more generally and the potential for its consequent over-representation in palaeoglaciological reconstructions (cf. Bennett & Evans, 2012; Eyles, 1979, 1983; Kjær & Krüger, 2001; Slomka & Eyles, 2015; Spedding & Evans, 2002).

The present study builds on the modern landsystem analysis of Evans et al. (2009) and Chandler, Chandler, et al. (2020). More specifically, we focus on surveying, charting and quantifying: (1) the development and collapse of partially supraglacial outwash fans that culminate in the appearance of outwash heads fronting depositional overdeepenings (Bennett & Evans, 2012; Price, 1969); and (2) the genesis of the ice-cored eskers that record the evolution of englacial drainage networks operating over such depositional overdeepenings (Bennett & Evans, 2012; Price, 1969; Spedding & Evans, 2002). This is significant more widely in that such localized, azonal and potentially intrazonal landsystem signatures (sensu Evans, 2013) are creating substantial ice-cored/hummocky terrains and this is likely to be replicated

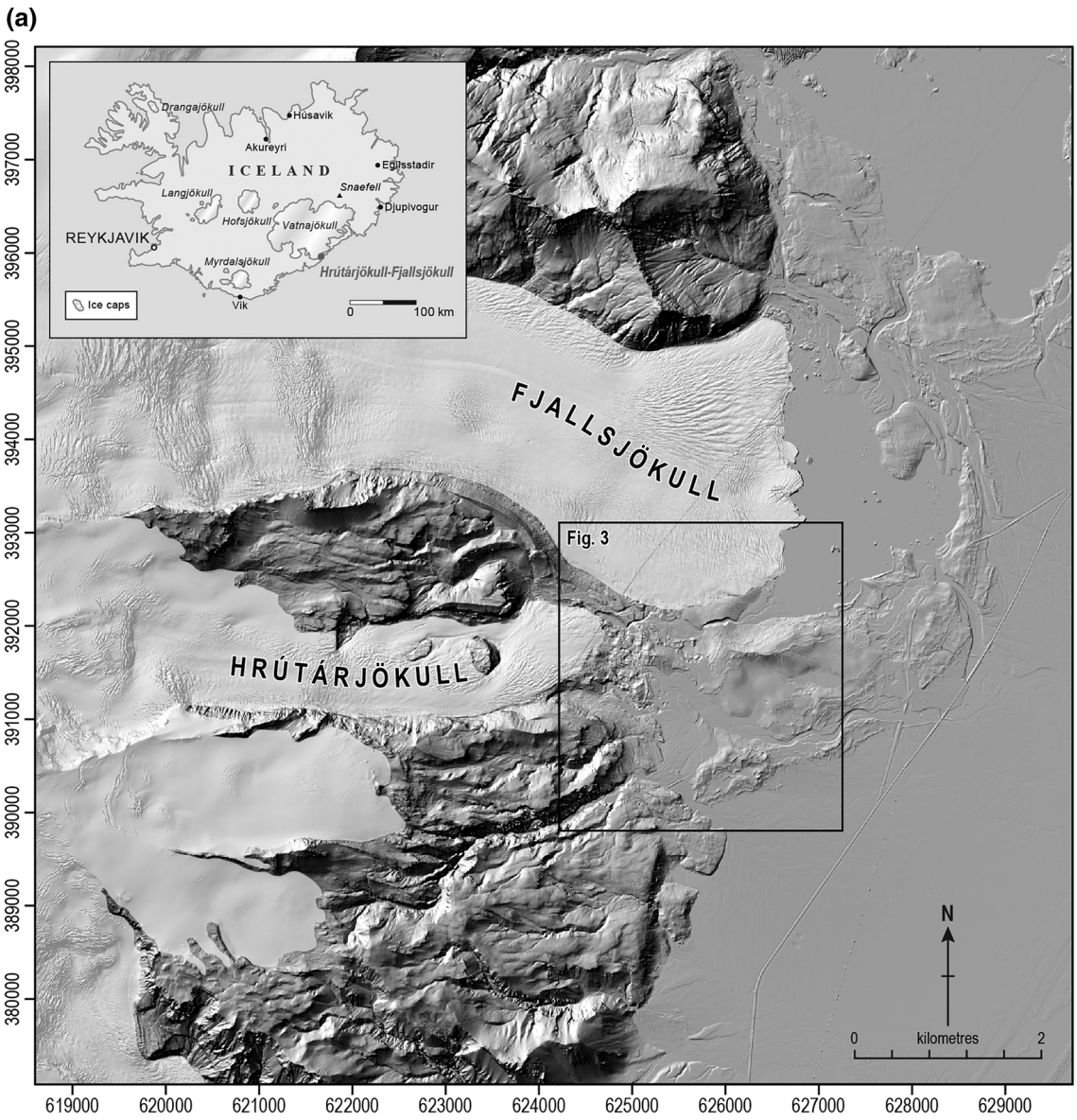

FIGURE 1 Location maps and glaciology of Fjallsjökull-Hrútárjökull: (a) LiDAR image of the Fjallsjökull-Hrútárjökull foreland with inset map showing the location of the study area in southern Iceland; (b) the Öræfi caldera and its ice cover with ice-marginal recession patterns and ages of the outlet glaciers mapped; (c) cross profiles (located in b) through the underlying topography and surface changes of the two snouts over time (from Hannesdóttir et al., 2015).

in the near future on deglaciating forelands in Iceland as well as further afield where ice-contact glacifluvial assemblages create outwash heads that act as depositional overdeepenings.

3 | METHODS

Systematic repeat mapping and landform characterization of rapidly deglaciating proglacial areas are essential for the development of our understanding and reconstruction of glacial process-form models and their relationships to glacier dynamics. However, the annual patterns of recession and the relatively small areas exposed every year mean that carrying out regular aerial or satellite surveying is expensive and impractical. Moreover, some of the landforms are very subtle, making it impossible to recognize them even with high-resolution satellite imagery (Ewertowski, Tomczyk, et al., 2019). Only recently, advances in technology have enabled the development of low-cost alternatives for traditional aerial surveys (Ewertowski, Tomczyk, et al., 2019; Hugenholtz et al., 2013; Smith et al., 2016; Westoby et al., 2012; Whitehead et al., 2014). Small uncrewed aerial vehicles (UAVs or drones) can be used to acquire high-resolution (several centimetre ground sampling distance [GSD]) low-altitude photographs. These UAV-based photographs can subsequently be processed using structure-from-motion (SfM) photogrammetry to generate detailed orthophotos and digital elevation models (DEMs). This very detailed, but spatially restricted, data can be combined with a coarser, but still high-resolution, satellite imagery to extend our interpretation to the scale of the whole forelands.

3.1 | Datasets and data processing

Historical development of the Fjallsjökull-Hrútárjökull foreland was reconstructed based on time series of archival aerial images covering

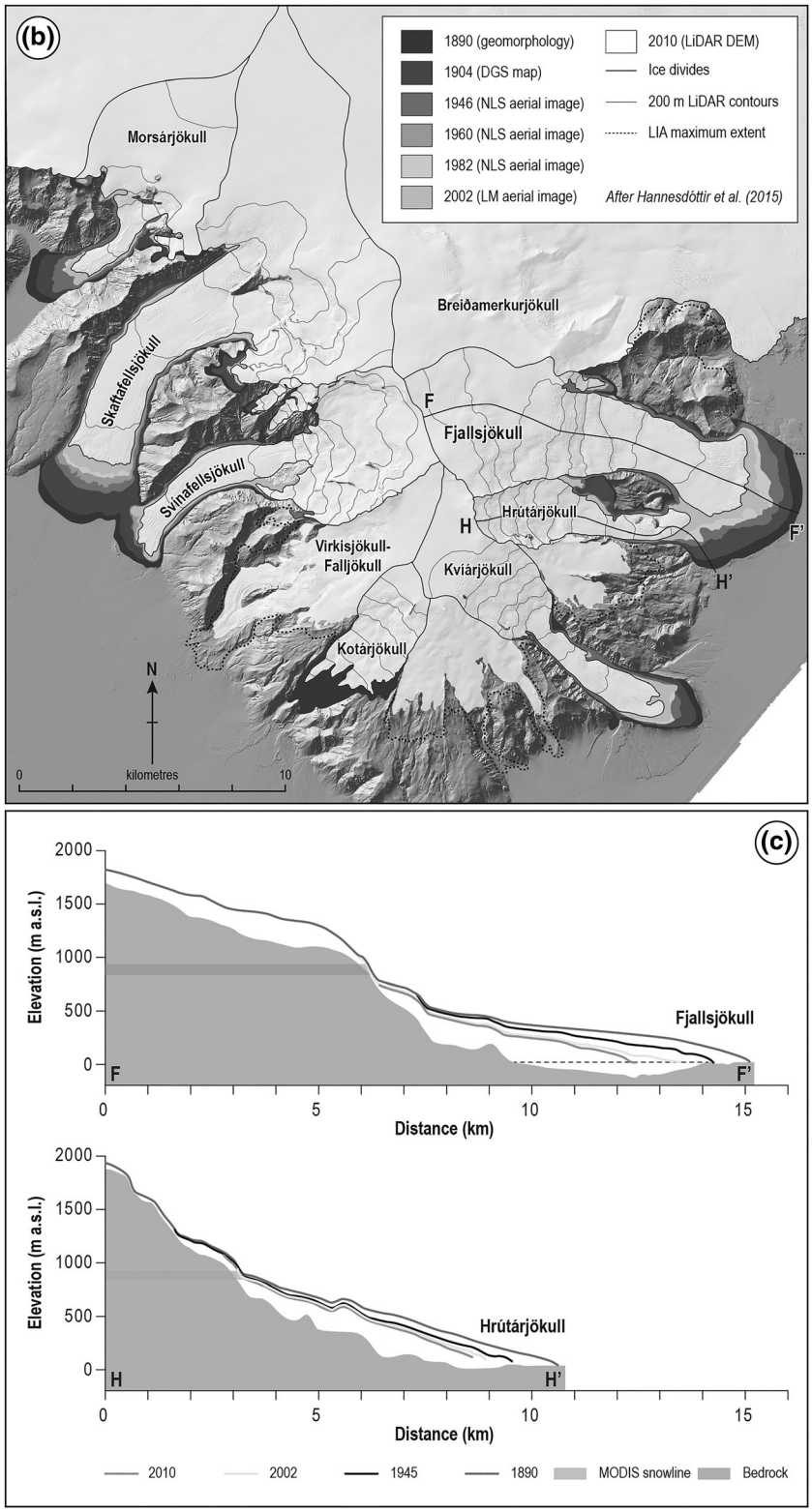

FIGURE 1 (Continued)

the period 1945–1998 and a high-resolution satellite image from WorldView-2 satellite captured on 23 September 2014. The satellite image was an ortho-ready standard product projected in ETRS89 UTM zone 28 N projection. The dataset was orthorectified and pan-sharpened to generate a four-band 0.5 m GSD multispectral product.

Detailed geomorphological mapping was based on the data collected using UAVs in 2014. Quantification of volumetric and areal changes was based on the time series of UAV data from 2014, 2016, 2018, 2019 and 2022 (Table 1). Flight operations were conducted at the end of August and the beginning of September each year. During each survey, ground control points (GCPs) were surveyed using differential GNSS Topcon Hiper II, with prominent stable features such as isolated boulders and small stone circles targeted as GCPs. The 2022 surveys were flown with a DJI Phantom 4 RTK, and the local GNSS

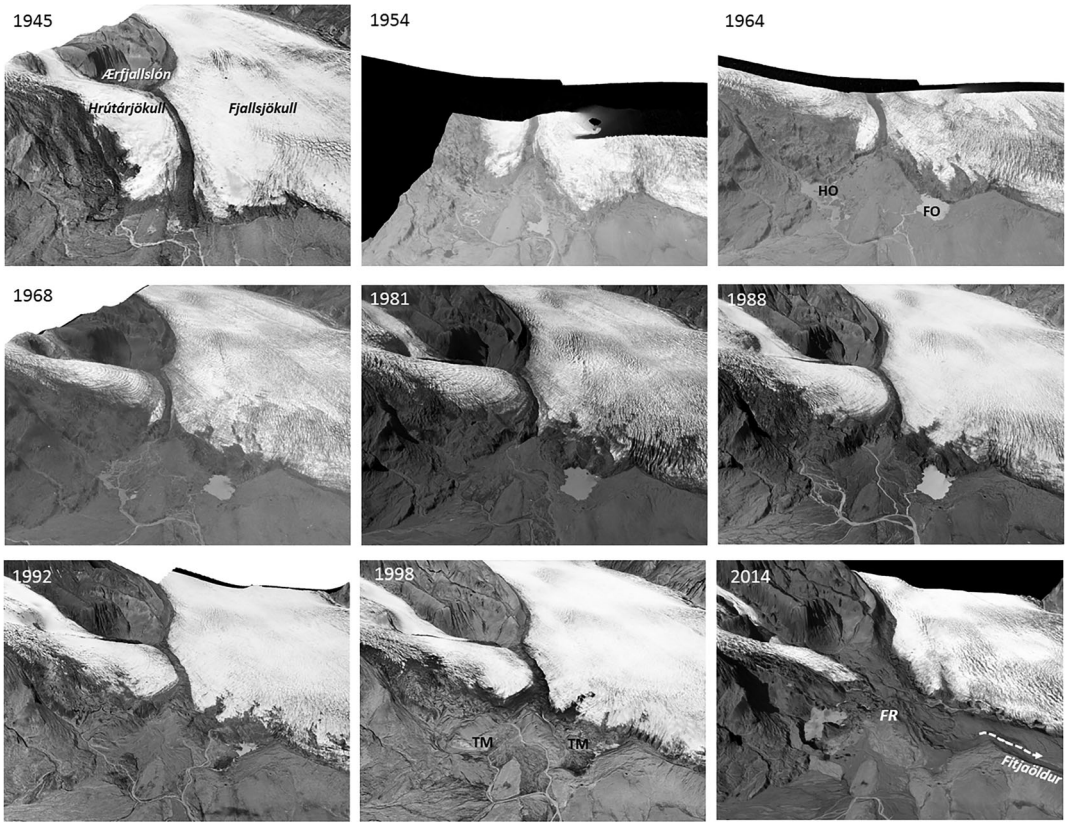

FIGURE 2 Oblique views over the Fjallsjökull-Hrútárjökull foreland for various dates using the available aerial photography and showing the changes in ice margins and proglacial landforms (aerial photographs by Landmaelingar Islands). HO = Hrútárjökull overdeepening; FO = Fjallsjökull overdeepening; TM = thrust moraine.

base station was run simultaneously to enable future processing of RTK camera positions.

Images captured by UAVs were processed using an SfM approach in Metashape Photoscan 1.8.4. We adopted the general approach as proposed by Evans et al. (2016) and generated dense point clouds, DEMs and orthomosaics. In addition, individual processing parameters were set up as indicated in the 'optimal' workflow for processing UAV data in Metashape (Śledź & Ewertowski, 2022). Following the approach proposed by Cook & Dietze (2019) and de Haas et al. (2021), we selected 2022 as a master model (because it was surveyed with RTK UAV) and co-registered each of the models with it.

3.2 | Quantification of landscape change

Quantification of landscape change focused on four key areas of the foreland, demarcated by boxes in Figure 4, in order to develop evolutionary sequences of landform–sediment assemblages (landsystem facets) as they relate to englacial meltwater processes and supraglacial outwash fan construction and collapse. Time series of UAV-generated DEMs were resampled to 0.1 m to ensure consistency of datasets from different years. DEMs of difference (DoDs) were constructed using Geomorphic Change Detection software (https://gcd.riverscapes.net/) as proposed by Wheaton, Brasington, Darby, Merz, et al. (2010) and Wheaton, Brasington, Darby and Sear (2010). This tool has been applied in previous studies in glacial environments (e.g. Chandler, Chandler, et al., 2020; Ewertowski, Evans, et al., 2019; Midgley et al., 2018; Tonkin et al., 2016). Errors were estimated based on stable surfaces (i.e. no changes were observed between sequential DEMs), with several areas selected for DEM pairs and used to investigate elevation differences. This provided an indicator of uncertainty, from which a 0.5 m elevation surface difference was established as a minimum level of change detection (minLoD).

3.3 | Geomorphological mapping

Geomorphological mapping of the former Fjallsjökull-Hrútárjökull coalescence zone (Figure 4) was undertaken following protocols outlined by Chandler et al. (2018) and conforming to cartographic styles of previous Icelandic foreland maps (see Evans, 2009 for an overview and references for case studies). Genetic classifications of landforms and sediments were based on interpretations of repeat aerial and satellite imagery as well as extensive field checking. The historical aerial photography was also employed to reconstruct the sequence of ice marginal change, lake development, meltwater and lake drainage and overall foreland evolution (Figure 2). The surficial geology units and landform symbology are compatible with previous maps by Evans et al. (2009) and Chandler, Chandler, et al. (2020), but with greater emphasis on the landform details of the depositional overdeepenings. The map (Figure 4) was produced at a scale of 1:1800 based on a 2014 orthophoto generated from UAV images.

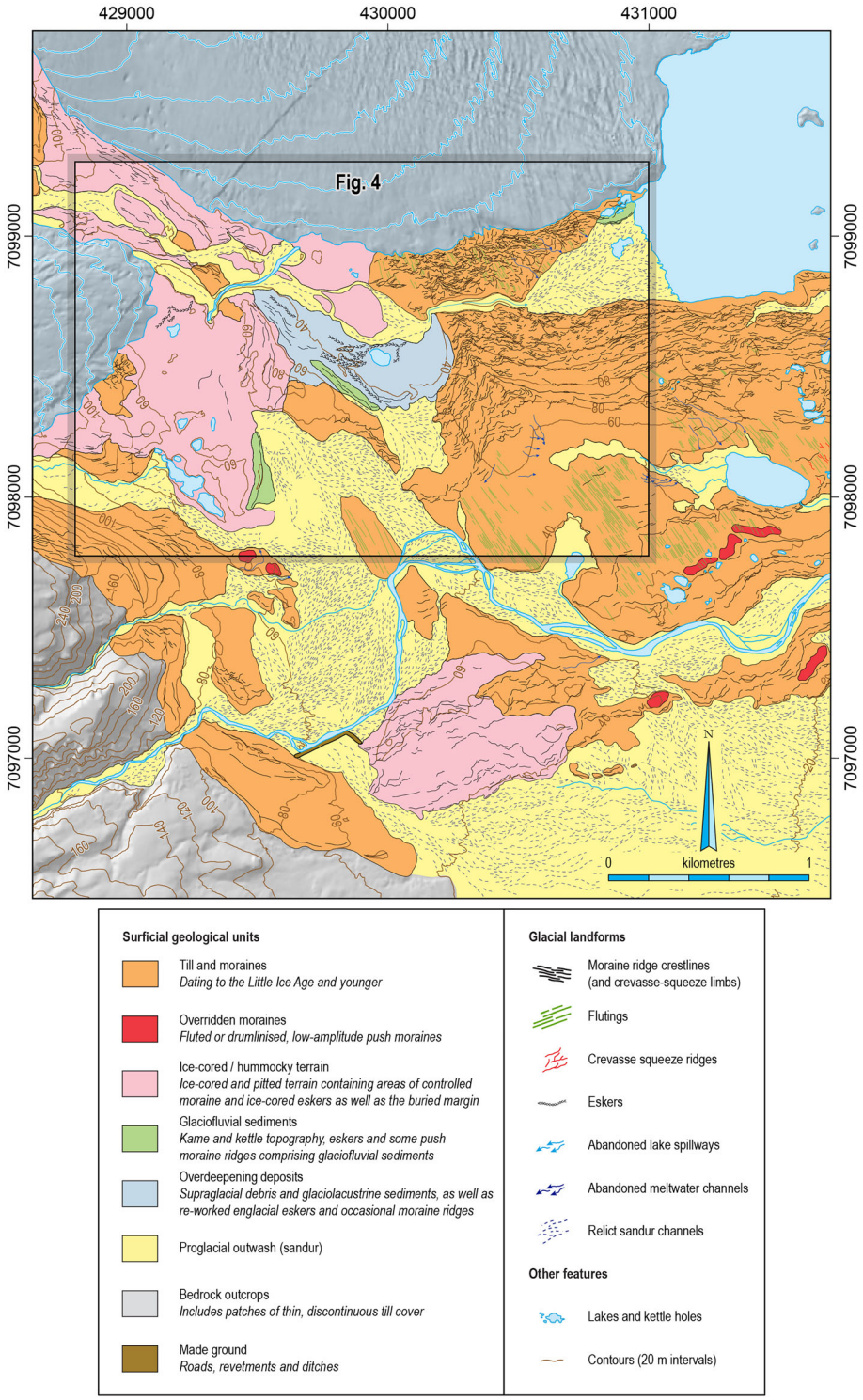

FIGURE 3 Extract from the surficial geology and geomorphology map of Chandler, Chandler, et al. (2020), showing the location of the study area in Figure 4.

TABLE 1 Aerial survey details

Date	UAV model	Sensor size (MP)	Focal length (mm)	Average flight altitude (m)	Number of images	Covered area (km^2)	GSD (cm)
2014 (Sep)	P2 Vision+	14	5	60	253	0.45	3.4
2014 (Aug/Sep)	Smartplane	12	5.2	100	2968	2.07	3.8
2016 (Sep)	P3	12	3.61	64	4346	2.18	2.8
2018 (Aug/Sep)	P4 Pro	20	8.8	106	4914	2.16	2.9
2019 (Sep)	P4 Pro	20	8.8	85	5764	2.81	2.3
2022 (Aug/Sep)	P4 RTK	20	8.8	97	7100	3.16	2.7

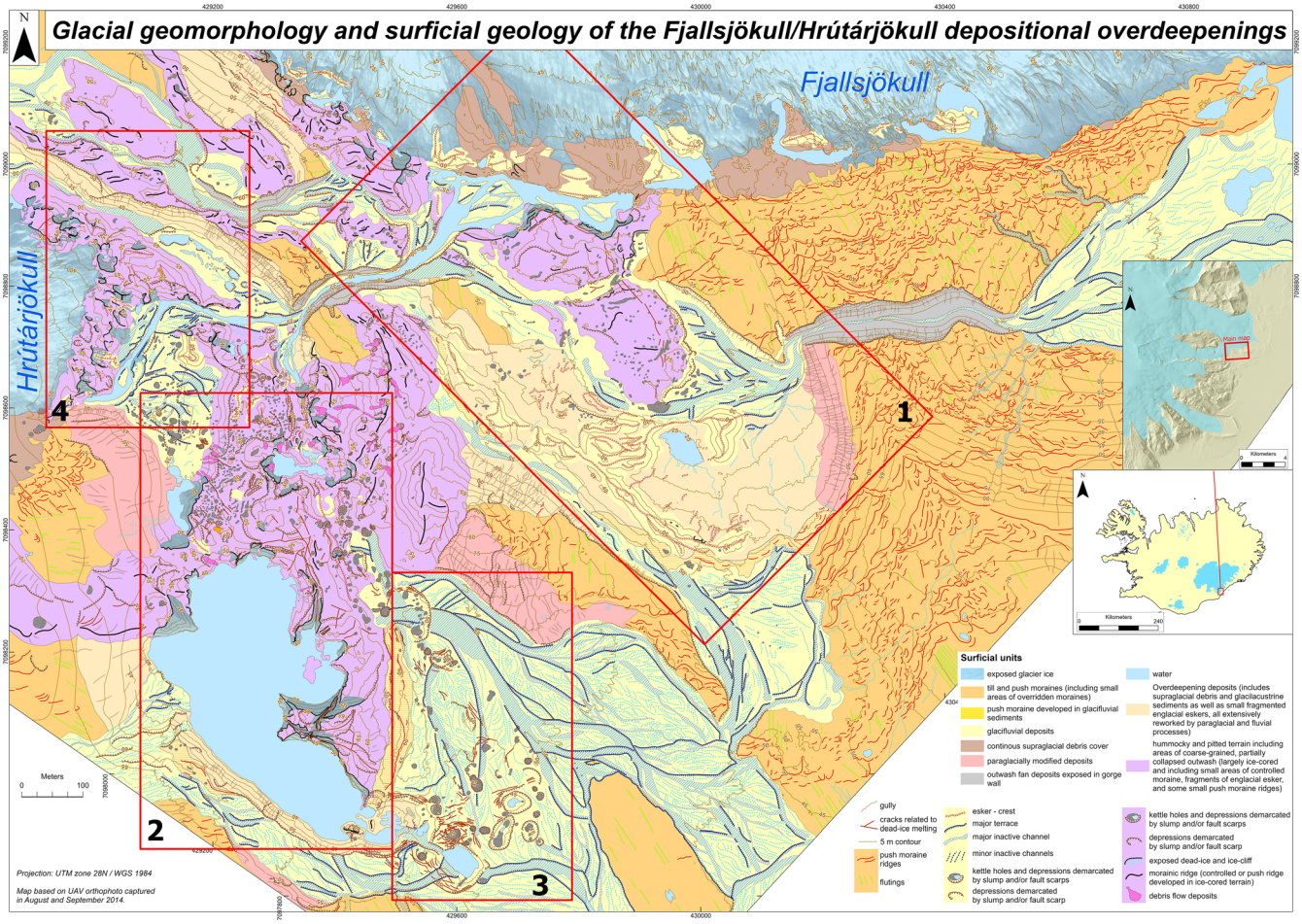

FIGURE 4 Surficial geology and geomorphology map of the study site, showing the details of landforms that have developed over the Fjallsjökull-Hrútárjökull foreland. Boxes show the coverage of the four case study areas.

4 | RESULTS

4.1 | Historical development of the Fjallsjökull-Hrútárjökull foreland and coalescence zone

In order to place the case studies presented here in the context of the wider foreland of Fjallsjökull-Hrútárjökull, we now provide a brief overview of historical glacier recession from the LIA maximum and the landforms charting that recession, as previously reported by Chandler, Chandler, et al. (2020) and Guðmundsson and Evans et al. (2022) and further augmented here by the observations on repeat aerial imagery. The process-form implications of this historical recession pattern are revisited in later sections.

The evolution of the landform–sediment associations of the Fjallsjökull-Hrútárjökull coalescence zone in particular can be charted from the first aerial photographs in 1945 (Figure 2). Initial recession of the snout from the LIA maximum moraines (dated to ca. 1890–1904 CE; Guðmundsson & Evans, 2022; Hannesdóttir et al., 2015) is recorded by closely spaced recessional push moraines, but in the 1930s and up until 1945, recession rates appear to have increased, as indicated by the foreland dating to that time being dominated by fluted till with more widely spaced moraines (Chandler, Chandler, et al., 2020; Evans et al., 2009; Guðmundsson et al., 2019). Outwash prograding from the snout in 1945 developed extensive linear sandar between upstanding areas of fluted till. At this time, the river Hrútá carried all the meltwater from the southern margin of the Fjallsjökull-Hrútárjökull lobe, augmented by runoff from the receding ice margins and mountains to the southwest in the river Múlakvísl (Guðmundsson & Evans, 2022). Overall glacier recession by around 1945 was beginning to uncover the large, arcuate and broad ridge of Fitjaöldur, which is up to 80 m high and superimposed by recessional moraines (Figure 2). The sedimentary core of Fitjaöldur is exposed in a spillway gorge, as documented by Chandler, Chandler, et al. (2020) and, together with its asymmetrical cross profile, reveals that this large arcuate feature is an overridden outwash head dating to pre-LIA times. The ridge likely formerly continued in a second arc across the Hrútárjökull foreland to join the hillslopes to the southwest. However, it has been dissected by glacial erosion during the LIA by the two glacier lobes, leaving an upstanding remnant (hereby the 'Fitjaöldur remnant') upon which the medial moraine between the two glaciers is now draped (Figure 2). A further gorge incised through this remnant reveals a coarse glacifluvial outwash sequence draped by medial moraine debris (Figure 5), confirming that it is part of the Fitjaöldur asymmetric ridge. Either side of this remnant lie the two overdeepenings in which our landform change case studies are located (Figures 3 and 4). As they are a product of the erosion of the Fitjaöldur ridge, they are technically erosional depressions but the enclosure of their southern ends by outwash heads creates their adverse slopes and hence we classify them as depositional overdeepenings.

FIGURE 5 The gorge through the Fitjaöldur remnant, revealing its internal stratigraphy of coarse glacifluvial outwash capped by medial moraine debris (above white dashed line). Note the inset nature of the terraces and their glacifluvial deposits (above yellow dashed line) that cross cut those of the remnant, indicating a depositional hiatus and hence no chronological relationship between terrace sediments and the Fitjaöldur stratigraphy. View looking towards the northwest from the surface of the Fitjaöldur remnant (see Figure 7b for location and view direction).

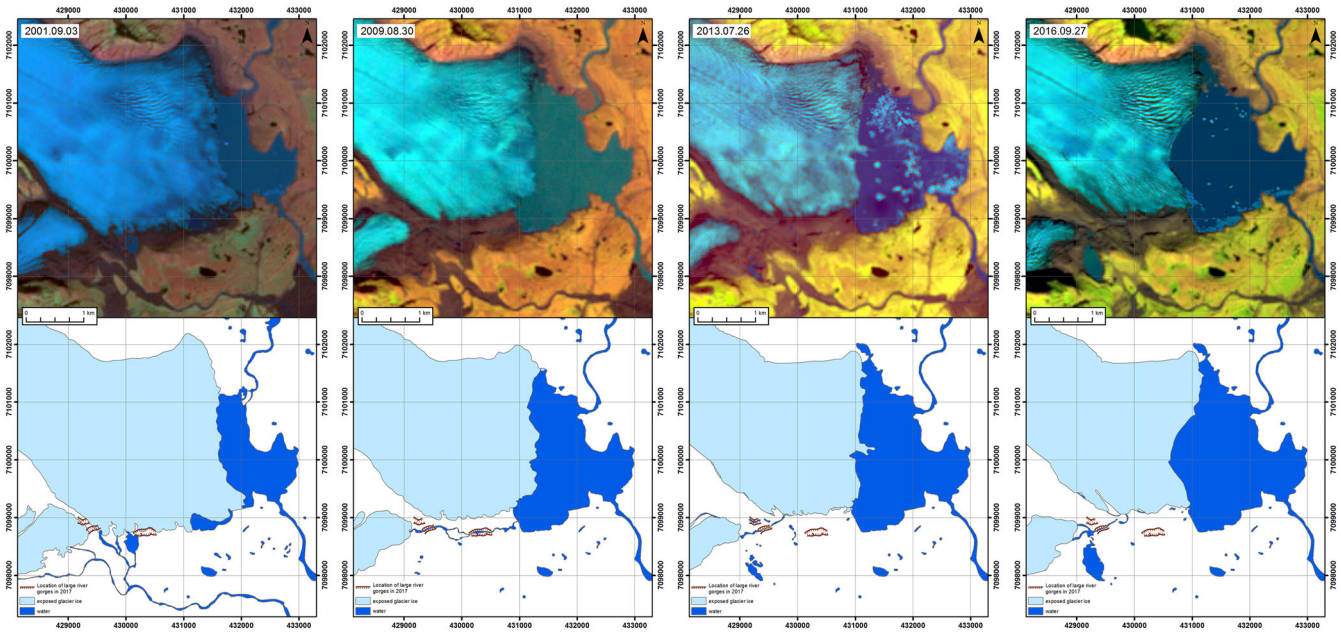

FIGURE 6 Changes in the major drainage pattern and lakes on the Fjallsjökull-Hrútárjökull foreland using satellite imagery for the years 2001, 2009, 2013 and 2016.

After 1945, the two glacier lobes began separating, developing a large area of medial moraine and debris-covered snout around the Fitjaöldur remnant, as evident in 1954 and 1964 aerial photographs (Figure 2). Similar substantial spreads of supraglacial debris were developing also along the right and frontal margin of Hrútárjökull, the latter lying over what has more recently been revealed as an overdeepening lying behind an outwash head (see case studies 2–4 below). The Fjallsjökull snout was marked by a series of controlled moraines aligned sub-parallel to the ice margin (ice flow-transverse) in 1954 and then further, ice flow-parallel supraglacial ridges that narrowed up-glacier in images from 1964 to 1998. The ice flow-parallel debris ridges developed sinuous plan forms from 1964 onwards, appeared lighter in colour and were cross-cutting the ice flow-transverse debris bands/ridges (Figure 2). This change in orientation, debris colour and cross-cutting characteristic reflects the development of englacial eskers, fed by debris from the transverse debris bands. As demonstrated by Chandler, Chandler, et al. (2020), the eskers gradually evolved into ice-margin parallel features once the Fjallsjökull snout had receded far enough down the steeper proximal slope of Fitjaöldur to allow sub-marginal meltwater drainage to flow towards Fjallsárlón. This eastward drainage direction, carrying the meltwater from the uncoupled Fjallsjökull and Hrútárjökull snouts, was initiated by the incision of the Fitjaöldur spillway in 2003–2004, when the remaining lake water in the Fjallsjökull overdeepening catastrophically drained and switched the flow direction of the river Hrútá (Figure 6).

As early as 1954, a large area of pitted outwash characterized the area of the downwasting debris-covered Hrútárjökull snout (Figure 2). By 1964, this area of pitted outwash had expanded northwards into the re-entrant that was forming between the uncoupling glacier snouts; at the Fjallsjökull part of the snout, an overdeepening was responsible for the growth of a proglacial lake behind the 1945 moraine arc (Figure 2). This lake persisted until 1989, at which time it had been reduced in size by the progradation of an outwash fan from

the northwest. Throughout this period of post-1930s snout recession, meltwater drainage was flowing southwards from the downwasting ice margins and then eastwards along the Hrútá, where its course was directed by the LIA maximum moraine arc (dating from ca. 1890–1930s CE; Guðmundsson & Evans, 2022; Figure 2). The 1992 and 1994 aerial images capture the continued infilling of the Fjallsjökull proglacial lake by the growth of the pitted outwash fan and the establishment of a braided stream network that drains southwards towards the linear sandar. Continued recession by the Hrútárjökull snout from 1964 to 1994 resulted in the northward expansion of the proglacial outwash as a narrowing corridor fed by meltwater debouching from an expanding area of debris-covered ice on the right frontal area of the glacier (Figure 2).

After 1994, significant changes took place at the margins of both glaciers as, like most other snouts in southern Iceland, they readvanced and constructed prominent moraines (Evans & Hiemstra, 2005; Evans et al., 2009, 2016, 2017a, b). This appears to have been driven by a combination of a ca. 5 year-long, positive North Atlantic Oscillation index and a post-1965–1990s long-term cooling trend (Evans, Guðmundsson, et al., 2019; Sigurðsson et al., 2007). Between the aerial images taken in 1994 and 1998, a clear impact of this readvance is the emergence of an area of glacitectonic thrust blocks from the pitted outwash fan that was infilling the Fjallsjökull proglacial lake (Figure 7a). This constructional terrain indicates that the glacier snout had readvanced, thrusting up an area of stagnant ice that lay underneath the ice-proximal part of the fan, and was slowly melting out to form kettle holes. By 2014, when the area was captured by satellite imagery, this area of thrust blocks had evolved into a complex sequence of ice-cored eskers lying inside a kame terrace that linked to the surface of a proglacial fan (Figure 7a; see case study 1 below). The eskers now form a broadly arcuate but complex sequence that drapes the ice-contact face of the fan and the floor of the overdeepening, with the highest elevation esker linking to the pitted lip of the ice-contact face (Figure 4).

The impact of the early 1990s readvance on the Hrútárjökull snout is manifested in the construction of a single push ridge, fronted by a crescentic-shaped proglacial thrust mass or composite glacitectonic thrust moraine composed of outwash deposits (Figure 7b). This outwash was part of the northerly narrowing sandur corridor that had previously developed between the snout and the Fitjaöldur remnant. On post-2014 aerial imagery, this 1990s readvance moraine complex was gradually partially consumed by buried ice melt-out and lake development (see case study 2 below) but the proglacially thrust outwash continues to be recognizable by its surface relict channels. The development of surface tension cracks and collapse pits is also increasingly evident, indicative of an ice core and hence a supraglacial origin for the former sandur corridor.

In 1998, the remnants of the south Fjallsjökull proglacial lake appear to be partially interlinked and are predominantly supraglacial ponds, lying mostly within a small push moraine that is linked to the thrust blocks; the push moraine has been constructed on the lip of the ice-contact face of the fan. Satellite imagery for 2001 reveals a substantial lake in this location, which has disappeared in the imagery for 2009, after the creation of the Fitjaöldur gorge (Figure 6). This documents the last stage of lake development over the south Fjallsjökull overdeepening, which was terminated by catastrophic drainage through a spillway in 2003–2004. Continued downwasting of the Fjallsjökull snout at this location resulted in the ongoing development of eskers in meltwater tunnels that migrated northwards and downwards through the ice, culminating with the glacier sub-marginal eskers that drain through the south Fjallsjökull snout towards Fjallsarlón (Chandler, Chandler, et al., 2020; Figure 7a). By 2001, satellite imagery shows that the Hrútárjökull drainage was also following this route, apparently after the initial incision of a further gorge through the Fitjaöldur remnant (Figures 5 and 6); the lake responsible for the full incision of this gorge was short-lived because the spillway was cut between imagery capture dates of 2001 and 2009 and must have formed largely supraglacially over the debris-covered snout on the northern end of the Hrútárjökull overdeepening. Not long after the incision of the gorge through the Fitjaöldur remnant, meltwater ceased to drain southwards over the long-established pitted outwash because of continued snout downwasting, especially at the south end of the Hrútárjökull overdeepening where the ice surface dropped below the emerging outwash head.

A significant change that took place in the area of the readvanced debris-covered snout of Hrútárjökull between 1998 and 2014 (Figure 7b) was the development of a large lake surrounded by steep cliffs in outwash deposits and remnants of debris-covered ice; this is the Hrútárjökull overdeepening which, unlike the south Fjallsjökull overdeepening, is still to be fully exposed by ice melt-out (Figure 2; see case study 2 below).

4.2 | Evolution of the glacial geomorphology of the Fjallsjökull-Hrútárjökull foreland and overdeepenings

Quantification of landform evolution in the Fjallsjökull-Hrútárjökull coalescence zone since 2014 is now exemplified through four case study areas (Figures 4 and 8). The first case study relates to the Fjallsjökull overdeepening and the other three to the Hrútárjökull snout and its overdeepening, but all four document the development of ice-cored glacifluvial landforms at downwasting active temperate piedmont lobes, interrupted by readvance moraine construction.

4.2.1 | Case study area 1: Landform development after lake drainage

Case study area 1 relates to the features that have emerged since the drainage of the former proglacial/supraglacial lake on the south Fjallsjökull margin in 2003–2004 (Figures 7a and 8–11), when catastrophic spillway incision of the Fitjaöldur gorge emptied the lake. As outlined above, the floor of the overdeepening, which is located inside an ice-contact fan, contains a complex assemblage of ice-cored, hence formerly englacial, eskers whose arcuate crestlines arc sequentially eastwards towards the spillway (Figures 9 and 10). Ice cores are proposed for these eskers because of the extensive development of contraction cracks, sink holes, damp patches on steep slopes and ongoing debris flow activity, all of which have been observed to become more widespread over field visits from 2014 to 2022.

The westernmost and highest-altitude esker lies directly downslope from a kame terrace and like the terrace feeds directly to the fan apex (Figure 11), indicating subaerial and englacial ice-marginal drainage to the fan after the construction of the ice-cored thrust

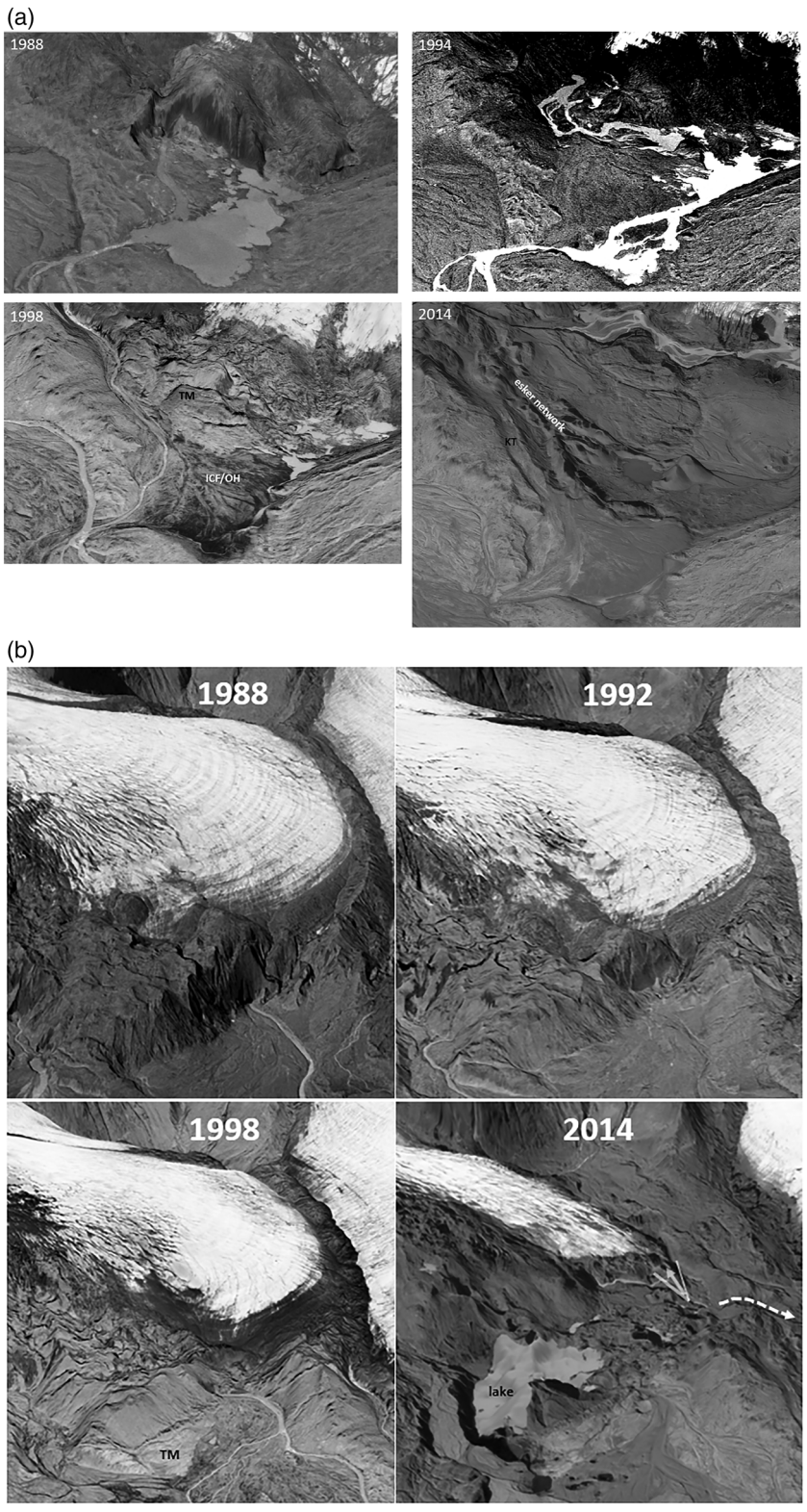

FIGURE 7 Oblique detailed views over the south Fjallsjökull (a) and Hrútárjökull (b) overdeepenings for various dates using the 1988–2014 aerial photography and showing the landform evolution associated with the 1990s readvance and later downwasting (aerial photographs by Landmaelingar Islands). TM = thrust moraine; ICF/OH = ice-contact fan/outwash head; KT = kame terrace. In (b), the dashed arrow marks the Fitjaöldur remnant spillway and the arrow and V symbol indicate the view in Figure 5.

blocks in the 1990s (Figure 7a). The inset sequence of the eskers in a downslope direction towards the overdeepening floor documents migration of the englacial drainage tunnels northwards and downwards through the ice, presumably during and after the 2004 lake drainage event. Notably, all up-ice ends of the eskers converge on a single location, specifically the former meltwater portal developed in the medial moraine zone visible on the 1988, 1994 and 1998 aerial photographs (Figure 7a). The esker emergence point converges on the upper cliffs of the gorge through the Fitjaöldur remnant, which was incised sometime between 2001 and 2009 (Figure 9). This suggests that the eskers were the product of sub-marginal and englacial tunnels excavated through the early 1990s readvance thrust moraine by the meltwater that initiated the early gorge incision. The origins of this water were likely from proglacial/supraglacial lake overflow from the debris-covered snout ice over the northern end of the Hrútárjökull overdeepening, which rapidly incised the gorge below the esker emergence point as the lake increased in size and the Fitjaöldur remnant emerged from the downwasting ice surface. This places the development period for the esker complex between 1998 (the culmination of the early 1990s readvance moraine construction) and 2003 when the

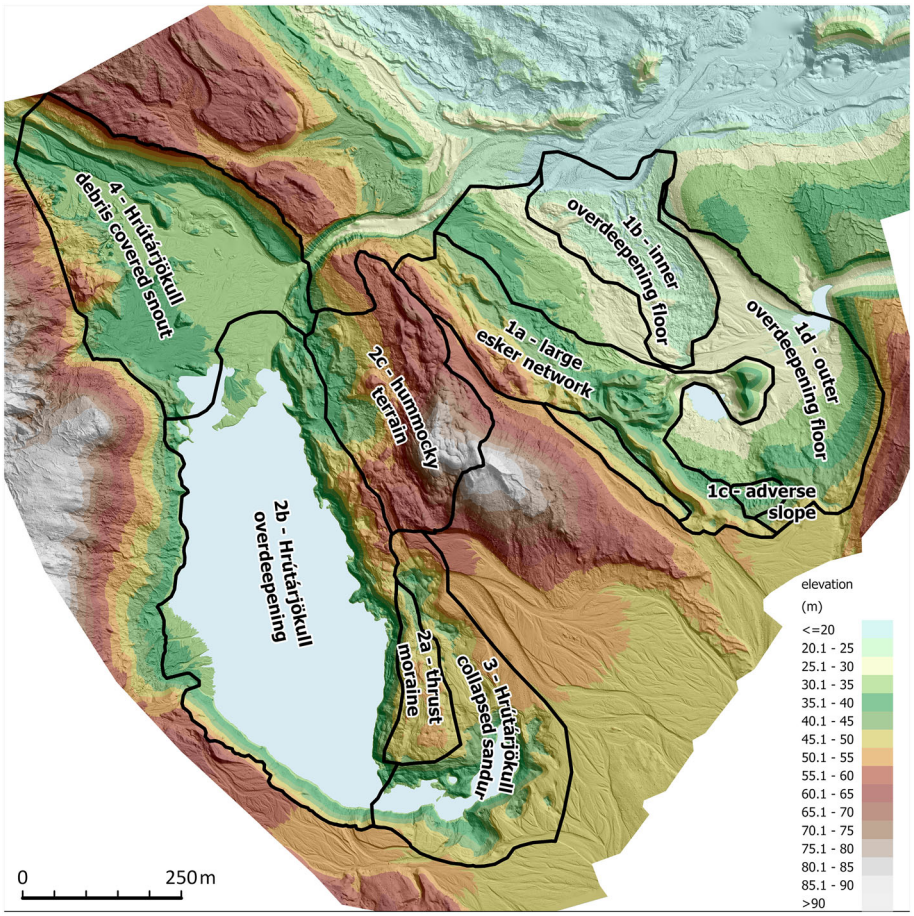

FIGURE 8 Elevation colour-coded DEM of the Fjallsjökull-Hrútárjökull foreland, showing the study areas sub-divided according to the areas used in recent landscape change calculations.

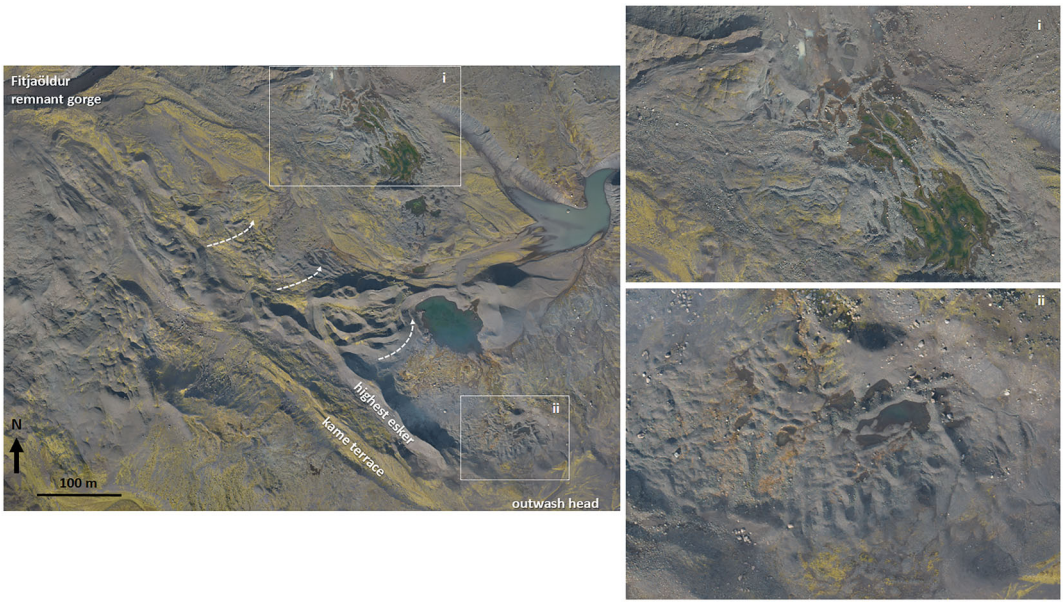

FIGURE 9 Extracts from the 2014 satellite imagery showing the eskers in the south Fjallsjökull overdeepening. Dashed arrows show general pattern of esker migration direction down through the ice overlying the overdeepening.

Fitjaöldur gorge drained the lake in the south Fjallsjökull overdeepening (Figure 6); a maximum of 5 years.

Two further complex networks of minor esker ridges and interlinked crevasse infills (short linear, gravel-filled ridges), predominantly aligned north–south, occur on the adverse slope of the outwash head (Figure 9ii) and on the inner floor of the overdeepening (Figure 9i). The former appear to record glacier sub-marginal drainage from the ice-contact fan surface back under the thinning snout and are therefore effectively subglacially or englacially engorged eskers (sensu Evans et al., 2018; Mannerfelt, 1945, 1949). The latter likely record the final englacial to subglacial and supraglacial infilling of tunnels and crevasses in the remnant glacier ice lying in the overdeepening, when

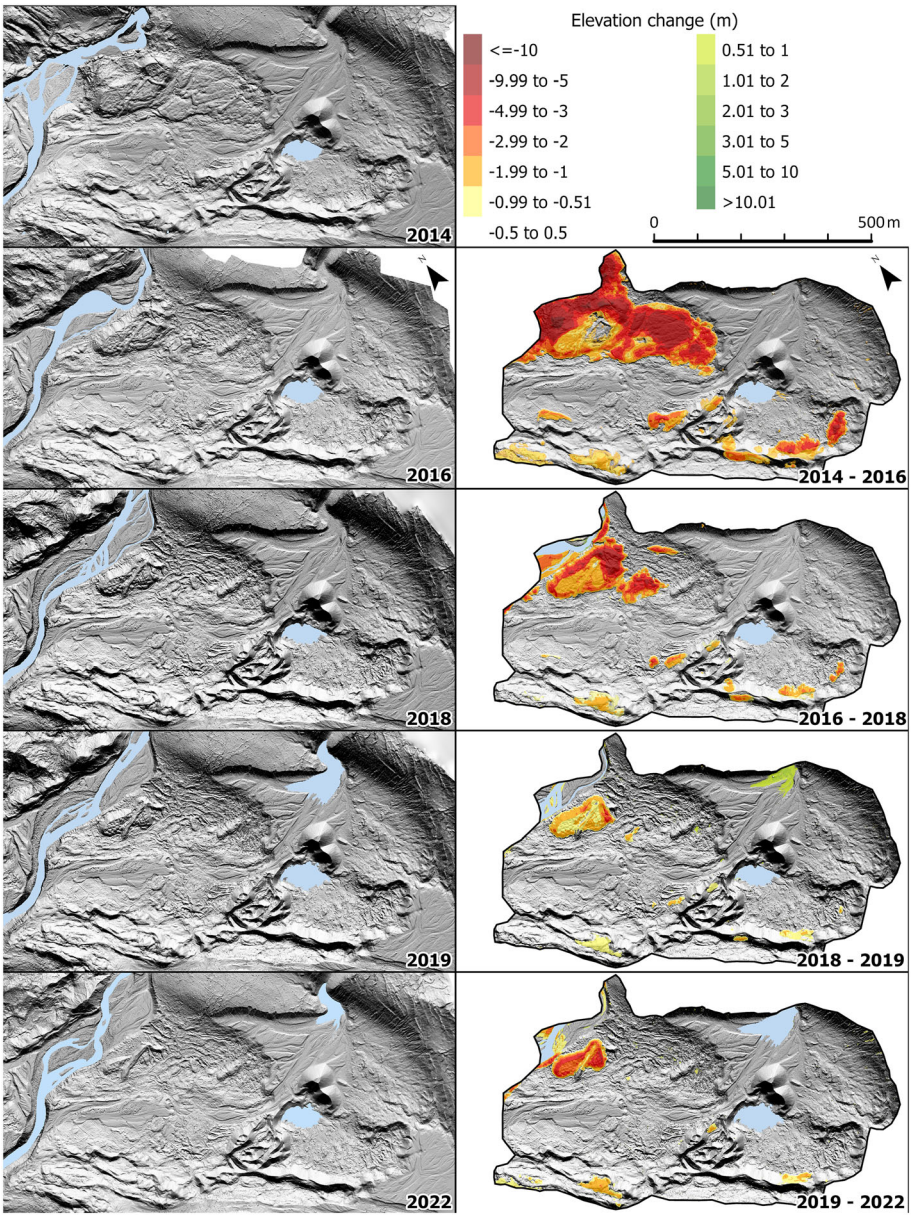

FIGURE 10 Hillshade models of case study area 1 (south Fjallsjökull overdeepening) for the years 2014, 2016, 2018, 2019 and 2022 (left panel) and DEMs of difference (right panel).

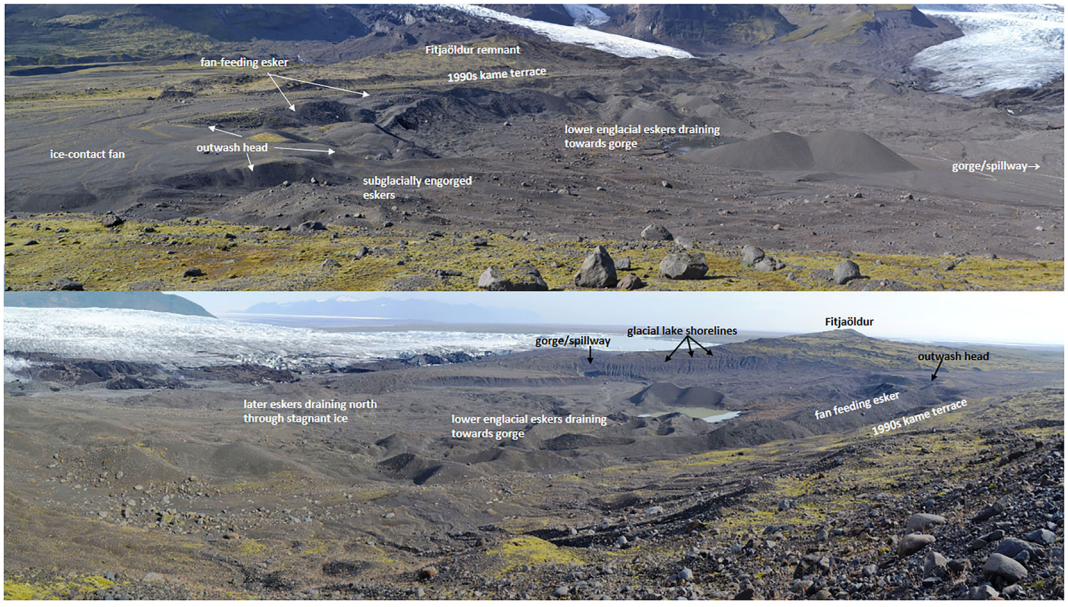

FIGURE 11 Ground views from 2014 looking west (upper) and east (lower) across the south Fjallsjökull overdeepening from the Fitjaöldur remnant with the main landforms identified.

drainage was directed back under the Fjallsjökull margin towards Fjallsarlón rather than through the spillway. The later stages of this process were observed in the field as late as 2016, when meltwater drainage through stagnant ice was cutting and filling tunnels that linked to the englacial eskers along the more restricted southern margin of the glacier, as documented by Chandler, Chandler, et al. (2020; Figure 12).

The more recent stages of evolution of these glacifluvial landforms are quantified using DEMs of difference (DoDs) for the years 2014, 2016, 2018, 2019 and 2022 (Figure 10; Table 2). The changes due to buried ice melt-out, as indicated by features such as tension cracks and sink holes, have since 2014 resulted in only minor adjustments of esker morphology, in contrast to the rapid annual developments recorded by Price (1969), Howarth (1971) and Storrar et al. (2015) for the Beiðamerkurjökull eskers. Detectable changes between 2014 and 2022 were recorded on 21 430 m^2 (28%) out of 77 850 m^2 of the area occupied by the main esker network. Despite being localized, some of the changes were substantial, with elevation lowering by up to 9.5 m on both sides of the esker ridges (total net volume difference −46 400 m^3 [±23%]). The more widespread transformation was recorded for the networks of minor esker ridges and interlinked crevasse infills located in the inner floor of the overdeepening. In 2014, this area was occupied by hummocky terrain covering approximately 51 560 m^2. Detectable changes in the period 2014–2022 were recorded in more than 86% of this area, and the total net volume change was −252 760 m^3 (±9%). As the terrain lowered over the years (in some places by up to 15.5 m; average elevation loss of 5.0 m), new eskers and crevasse infills emerged from this hummocky terrain. A lower degree of transformation (57% of the area; maximum elevation lowering up to 9 m; average elevation lowering 2.0 m) was observed for the network of minor ridges located on the adverse slope of the outwash head, where the total net volume change was −6940 m^3 (±14%).

Taking into account the whole of case study area 1 (269 800 m^2), the detectable changes (i.e. >0.5 m) between 2014 and 2022 were observed for 27% of the area. The total volume loss for the whole of case study area 1 in the period 2014–2022 was approximately 317 520 (±11%) m^3; a small volume of surface increase (180 m^3 [±77%]) was mostly related to deposition at the foot of the escarpment. The average change in the surface elevation for the area with detectable changes in elevation was −4.4 m (Figure 13a). The rate of change was fastest in the first observation period (2014–2016; Figure 13b); as the dead ice melted out, the rate of change then diminished. Between 2019 and 2022, detectable changes were recorded only on 5% of the area, amounting to a net volume difference of −21 690 m^3 (±31%).

4.2.2 | Case study area 2: Ice melt-out in the Hrútárjökull overdeepening

Case study area 2 relates to the uncovering of the Hrútárjökull overdeepening by large-scale ice melt-out between 2009 and 2014. This produced a large lake bounded to the southwest by steep cliffs in outwash deposits and, to the north and east, in ice-cored hummocky terrain and the remnants of the early 1990s pitted thrust moraine (Figures 7b, 14 and 15). This is mostly replacing large areas of debris-covered ice that had developed at the right lateral and frontal margin of Hrútárjökull and that had thickened and readvanced in the early 1990s (Figures 2 and 7b). The outwash deposits to the southwest were previously formed in an ice-marginal braided stream lying at the base of a steep debris-covered ice cliff and now constitute a kame terrace after the removal of the debris-covered ice; this terrace links directly to the sandur surface to the south.

The evolution of this large lake and its surrounding landforms is quantified using DoDs for the years 2014, 2016, 2018, 2019 and 2022 (Figure 14; Table 2). In 2014, the lake covered 83 633 m^2. Between 2014 and 2016, large areas of dead ice degraded and the lake area increased to 136 731 m^2. After 2016, the lake area continued to increase, but by a smaller amount, to 145 619 m^2 in 2022. A much higher range of uncertainty characterizes elevation and volume change calculations for case study area 2 because of the variations in lake water level. Nevertheless, the recorded changes were substantial. The total area covered by the lake and ice-cored moraine/debris-covered snout in 2014 was 250 750 m^2. Between 2014 and 2022, elevation changes were recorded in almost 90% of this area. The total net volume difference was −1 335 460 m^3 (±5%). Maximum elevation loss was 29.5 m, and average elevation lowering was 6.3 m. The changes were related to dead-ice degradation and lake expansion. Again, changes were the most rapid in the first observation period (2014–2016) when the majority of dead ice disintegrated (net volume loss 996 823 m^3 [±5%]; average elevation change of −4.7 m). Subsequent evolution was slower and related to the degradation of the lake shorelines and melting out of the remaining part of the ice-cored terrain. The total net volume changes for case study area 2 were −485 650 m^3 (±15%) for the period 2016–2018, −113 600 m^3 (±35%) for 2018–2019 and 45 970 m^3 (±29%) for 2019–2022.

FIGURE 12 Residual glacier ice on the floor of the south Fjallsjökull overdeepening in 2014, with a meltwater tunnel draining northwards, back towards the receding snout.

TABLE 2 Calculations of total volume change using DoDs as a surrogate for buried ice lost to melt-out over time since 2014 (panel a) and average elevation loss (normalized by area) = surface lowering volume divided by case study area (m^3/m^2) (panel b)

Panel a		Volume change (m^3)				
Case study area	Area (m^2)	2014–2016	2016–2018	2018–2019	2019–2022	Total(2014–2022)
1 – south Fjallsjökull overdeepening, including:	268 800	221 530 (±32%)	66 570 (±22%)	11 220 (±47%)	21 690 (±31%)	317 520 (±11%)
1a – large esker network	77 850	26 340 (±58%)	8140 (±43%)	2250 (±67%)	3820 (±47%)	46 400 (±23%)
1b – inner overdeepening (hummocky terrain in 2014)	51 060	183 280 (±13%)	55 030 (±19%)	8730 (±41%)	15 280 (±25%)	252 760 (±9%)
1c – adverse slope	3540	7120 (±24%)	940 (±29%)	80 (±54%)	2 (±75%)	6940 (±14%)
1d – outer overdeepening	136 350	4790 (±20)	2460 (±23%)	160 (±57%)	2590 (±46%)	11 380 (±16%)
2a – Hrútárjökull 1990s thrust moraine	18 650	46 120 (±20%)	37 180 (±24%)	19 860 (±44%)	40 000 (±32)	143 890 (±6%)
2b – Hrútárjökull overdeepening	212 610	996 823 (±5%)	485 650 (±15%)	113 600 (±35%)	45 970 (±29%)	1 335 460 (±5%)
2c – Hrútárjökull hummocky terrain/ medial moraine	72 740	141 060 (±25%)	57 780 (±38%)	25 340 (±55%)	69 790 (±31%)	297 790 (±11%)
3 – Hrútárjökull collapsed sandur	80 870	135 790 (±29%)	78 410 (±23%)	39 550 (±37%)	62 840 (±25%)	297 360 (±9%)
4 – Hrútárjökull debris-covered snout	130 820	N/A	114 970 (±14%)	127 190 (±23%)	347 540 (±10%)	517 930 (±11%) (2016–2022)

Panel b	Average elevation loss (m)				
Case study area	2014–2016	2016–2018	2018–2019	2019–2022	Total(2014–2022)
1 – south Fjallsjökull overdeepening, including:	0.8	0.2	0.0	0.1	1.2
1a – large esker network	0.3	0.1	0.0	0.0	0.6
1b – inner overdeepening (hummocky terrain in 2014)	3.6	1.1	0.2	0.3	5.0
1c – adverse slope	2.0	0.3	0.0	0.0	2.0
1d – outer overdeepening	0.0	0.0	0.0	0.0	0.0
2a – Hrútárjökull 1990s thrust moraine	2.5	2.0	1.1	2.1	7.7
2b – Hrútárjökull overdeepening	4.7	2.3	0.5	0.2	6.3
2c – Hrútárjökull hummocky terrain/medial moraine	1.9	0.8	0.3	1.0	4.1
3 – Hrútárjökull collapsed sandur	1.7	1.0	0.5	0.8	3.7
4 – Hrútárjökull debris-covered snout	N/A	0.9	1.0	2.7	4.0 (2016–2022)

Note: The column 'Total (2014–2012)' is not a simple sum of the remaining three columns, because: (1) changes in subsequent periods (2014–2016, 2016–2018, etc.) might be below level of detection, but for the whole 2014–2022 some of them will be large enough to be detected, and hence the 2014–2022 change will be larger than the sum of individual periods; (2) in some case studies (especially 2b – Hrútárjökull overdeepening) the 2014 image does not cover the whole area, and therefore the volume of change for 2014–2022 will be lower than the sum of individual periods.

4.2.3 | Case study area 3: Pitting and collapse of proglacial outwash

Case study area 3 relates to the extensive pitting and widespread collapse of the proglacial outwash immediately fronting the debris-covered snout of Hrútárjökull as it appeared in 1998. This sandur had accumulated over the period 1964–1998 (Figure 2), a period when the glacier margin was relatively stable. Pits had appeared in this outwash surface on 2014 imagery and then gradually expanded through the development of inset concentric tension cracks, growing an arcuate depression that linked to the lake in case study area 2 in 2022 (Figures 2, 4, 16 and 17). Additionally, this widespread collapse of the sandur surface, as indicated by the growth of tension crack networks, continued into the ice-cored hummocky terrain as well as the early 1990s push-moraine ridge and pitted thrust moraine on the east side of the lake (Figure 17). This indicates that the sandur of pre-1990s readvance age was ice-cored and deposited over shallow snout ice during a period of relative snout stability before the readvance occurred. As highlighted above, this stable period started around the mid-1960s and culminated in the early 1990s readvance (Figures 2 and 7b; Evans, Guðmundsson, et al., 2019; Sigurðsson et al., 2007) and followed a phase of apparently rapid recession from the late 1930s to 1945 (Guðmundsson & Evans, 2022).

The evolution of this area of outwash collapse is quantified using DoDs for the years 2014, 2014, 2016, 2019 and 2022 (Figures 13 and 16; Table 2). In 2014, the 1990s thrust moraine covered an area of 18 650 m^2 and the collapsing part of the outwash had an area of 80 870 m^2. The thrust moraine underwent a rapid transformation,

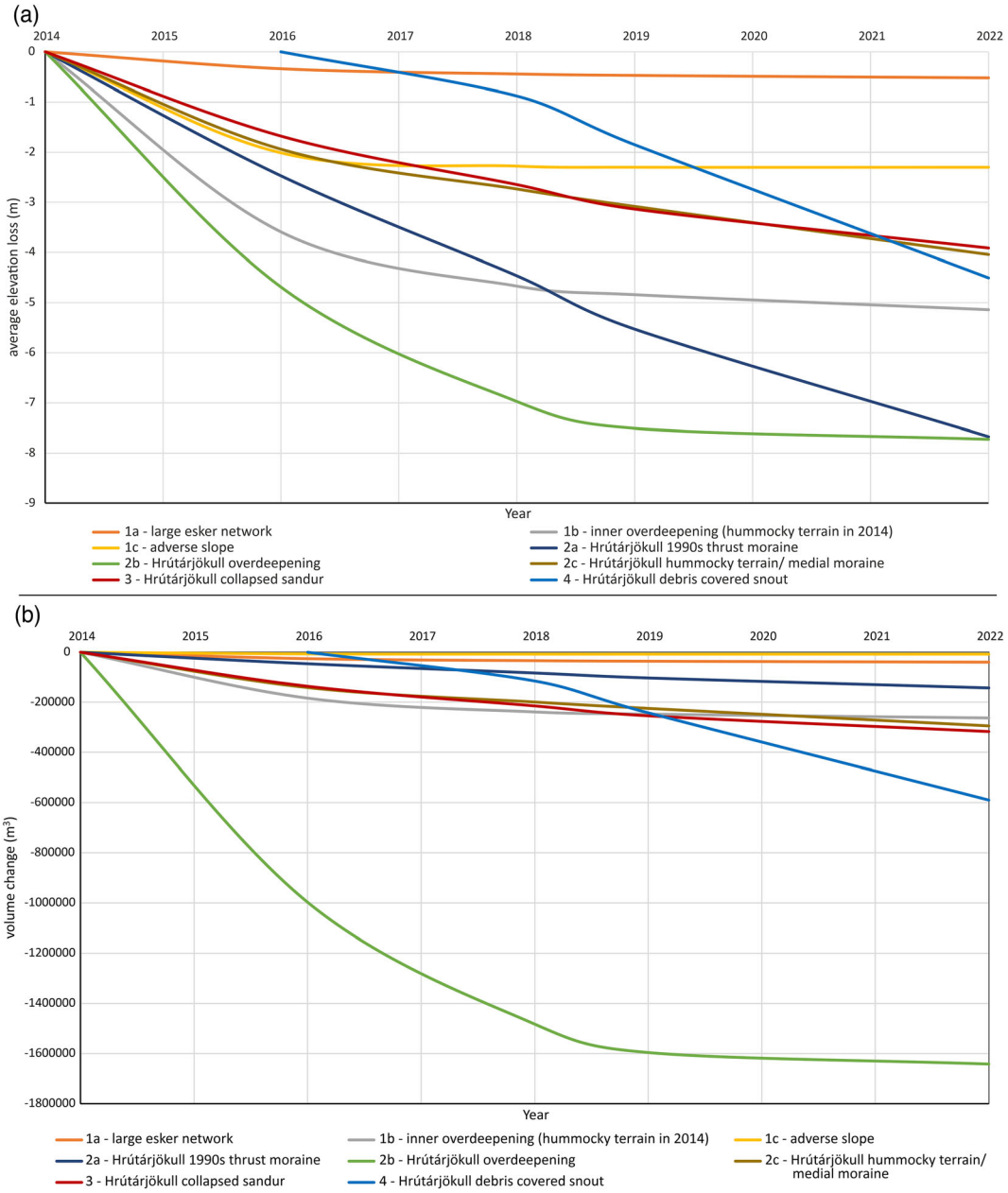

FIGURE 13 Graphs showing: (a) cumulative average elevation change (volume normalized by area); and (b) cumulative total volume change (m^3) in the different case study areas as defined in Figure 8.

collapsing towards the lake and downwasting. The total net volume change for 2014–2022 was −143 890 m^3 (±6%) and 100% of the moraine was subject to elevation loss higher than the detection level. The average elevation change for 2014–2022 was −7.7 m, with the highest values exceeding 15.5 m. In contrast with case study areas 1 and 2, which experienced the most change in the period 2014–2016, the thrust-moraine collapse was more or less uniform over time and volume loss was 46 120 m^3 (±20%) for the 2014–2016 period, 37 180 m^3 (±24%) for 2016–2018 and 40 000 m^3 (±32%) for 2019–2022.

The collapsed outwash in case study area 3 also degraded considerably, and net volume loss in 2014–2022 was 297 360 m^3 (±9%) for the area, with detectable changes occurring over 53 550 m^2. The average elevation loss was 3.7 m, with maximum values in places where new depressions were formed, reaching up to 15 m. Here, the biggest changes were observed for the period 2014–2016 (net volume loss 135 790 m^3 [±29%]) and, after 2016, transformations were somewhat slower: 78 410 m^3 (±23%) for 2016–2018; 39 550 m^3 (±37%) for 2018–2019; and 62 840 m^3 (±25%) for 2019–2022. Higher uncertainty values are once again related to the presence of water in collapsed depressions and changes in their water levels.

4.2.4 | Case study area 4: Evolution of a debris-covered snout

Case study area 4 relates to the area of debris-covered snout on the northern frontal margin of Hrútárjökull (Figure 18). The 2014 map (Figure 4) captures the stage of development when pitted outwash had replaced areas of debris-covered snout. This is manifest as a linear, terraced sandur between the north glacier margin and the

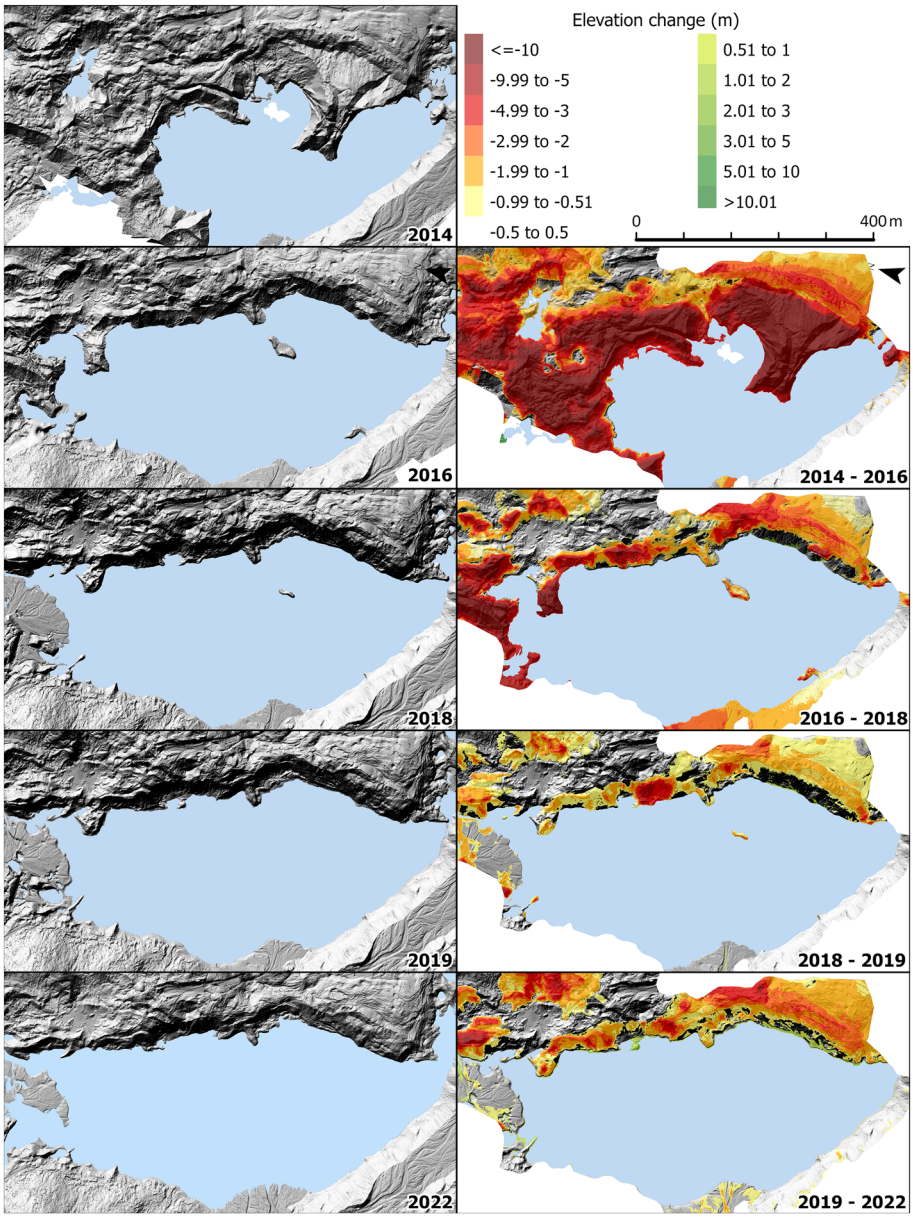

FIGURE 14 Hillshade models of case study area 2 (Hrútárjökull overdeepening) for the years 2014, 2016, 2018, 2019 and 2022 (left panel) and DEMs of difference (right panel).

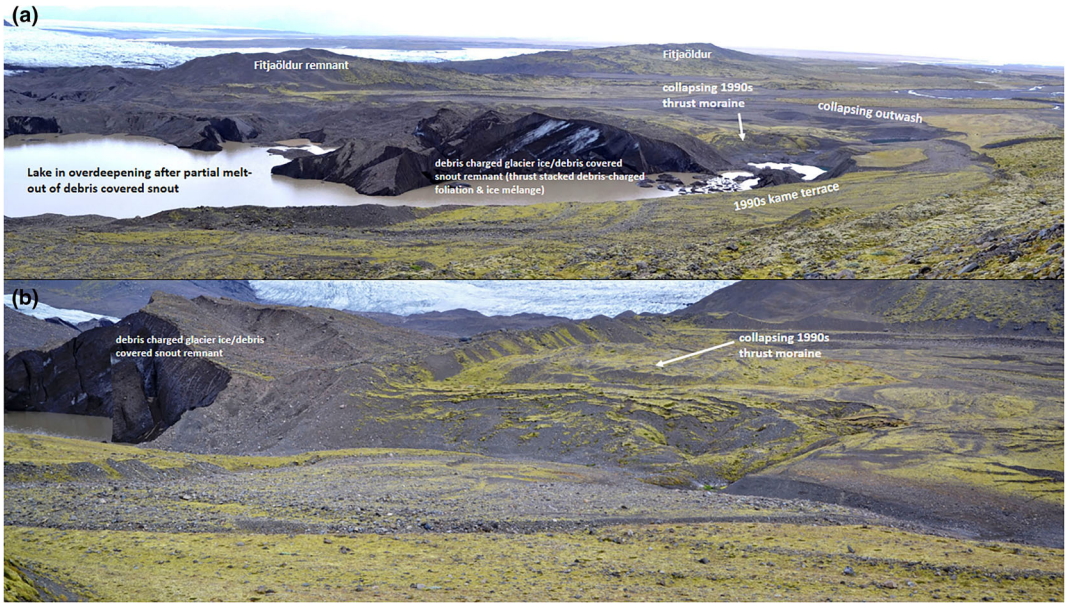

FIGURE 15 Ground views from 2014 looking east (a) across the Hrútárjökull overdeepening and north (b) across the remnant debris-covered snout and 1990s readvance moraine, with the main landforms identified.

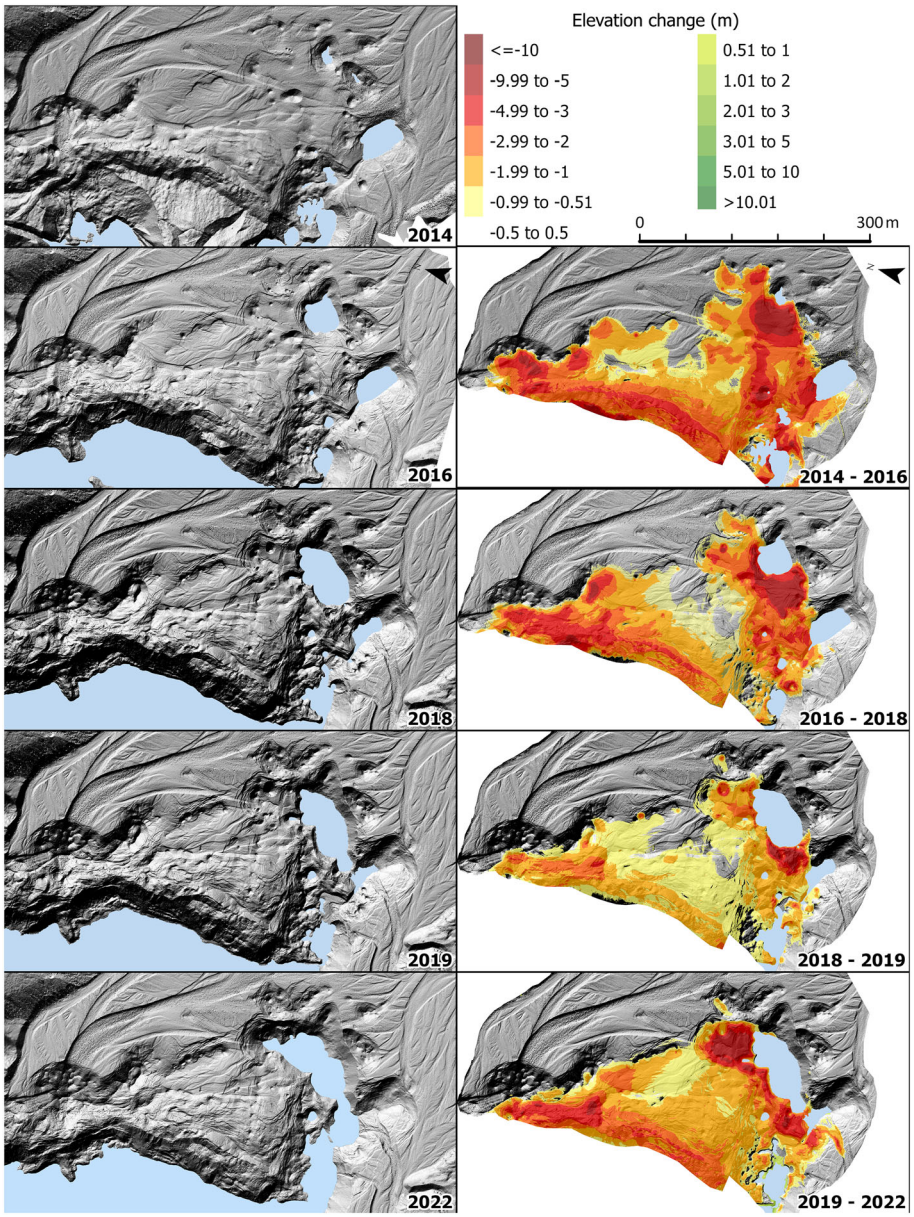

FIGURE 16 Hillshade models of case study area 3 (Hrútárjökull overdeepening south) for the years 2014, 2016, 2018, 2019 and 2022 (left panel) and DEMs of difference (right panel).

FIGURE 17 Ground view looking northeast (upper) and oblique aerial UAV view looking south of the collapsing outwash surface around study areas 2 and 3 in 2014.

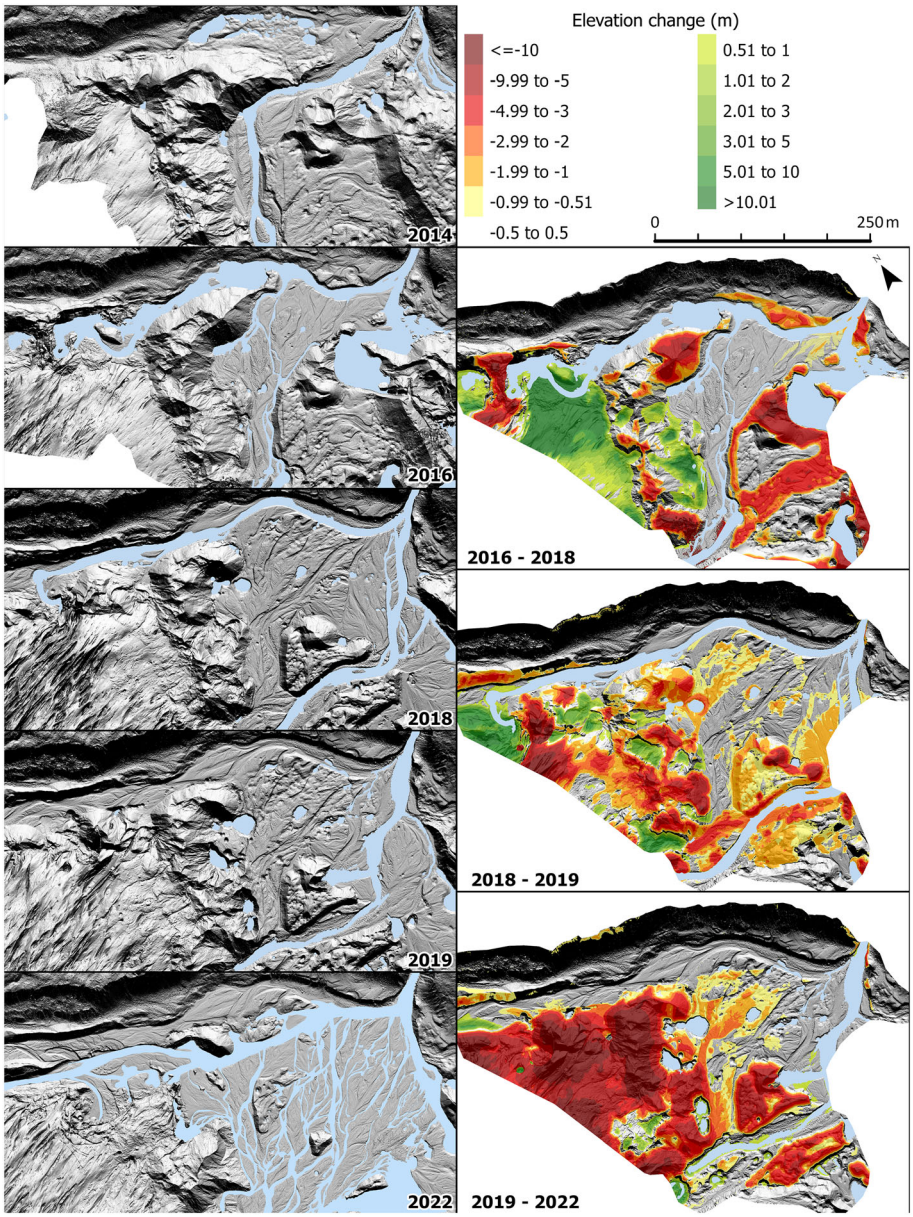

FIGURE 18 Hillshade models of case study area 4 (Hrútárjökull overdeepening north) for the years 2014, 2016, 2018, 2019 and 2022 (left panel) and DEMs of difference (right panel).

hillslope of the mountain interfluve between Hrútárjökull and Fjallsjökull, and as a sandur fan with its apex in the centre of the former snout, the positioning of which has been determined by the emergence of a bedrock high point through the downwasting glacier. Both of the sandar feed into and are modifying the northern end of the large area of detached debris-covered snout that lies over the Hrútárjökull overdeepening (see case study area 2). From 2014 onwards the river Hrútá emerges from the central part of the glacier snout and feeds the outwash fan before flowing through the gorge in the Fitjaöldur remnant, which was incised by proglacial/supraglacial lake overflow sometime between 2001 and 2009 (Figure 6; see also case study area 1). After the gorge was cut, the various supraglacial ponds and enlarging lake (case study area 2) drained northwards via a short tributary through the debris-covered stagnant snout ice and into the easterly flowing Hrútá.

The evolution of the outwash assemblages from imagery captured in 2014, 2016, 2019 and 2022 (Figure 18; Table 2) reveals generations of glacifluvial landform modification. In 2014, the linear sandur on the north side of the snout was terraced, recording the migration of the marginal river down towards the receding debris-covered ice margin, thereby creating kame terraces. The lowest river level had developed significant pitting, indicative of larger volumes of buried ice than earlier terrace remnants. By 2019, renewed aggradation by the ice-marginal river had resulted in the replacement of the lower, pitted surface with a largely undisturbed channelized river bed, but this had been displaced northeastwards by the expansion of the outwash fan, which had downcut and reworked upstanding areas of debris-covered ice; extensive kettling of the fan surface reveals that buried glacier ice persisted in 2019.

Quantification of the changes in this area of kame terrace and outwash fan development has been undertaken using DoDs for the years 2016, 2018, 2019 and 2022 (Figures 13 and 18). Time series of DEMs recorded a minor advance of Hrútárjökull in the period 2016–2018. The glacier margin advanced by up to 50 m, pushing an emerging esker into the previously constructed outwash. This advance was responsible for the volume gain of 255 960m^3 (±15%). During the same period, the ice-cored eskers and kettled terraces continued to melt, which is recorded by the volume loss of 114 970 m^3 (±14%). Between 2018 and 2019, the advance continued, albeit at a slower pace, and the ice margin advanced by less than 10 m. The total

volume increase related to this advance was +43 180 m^3 (±21%). Glacier ice and ice-covered landforms had already started degrading, and changes related to the collapse of outwash were also recorded, translating into a volume loss of 127 190 m^3 (±23%). Over the period 2019–2022, most of the ice that advanced in 2016–2019 melted. Further degradation and collapse of outwash and hummocky terrain was also recorded. Volume loss in 2019–2022 was 347 540 m^3 (±10%). The average value of surface lowering was 4 m, but in some places where the clean glacier ice melted, the elevation change was as much as −25.5 m during these three years. In contrast, a slight increase in volume was recorded for some areas over the 2019–2022 period as a consequence of drainage pattern change and new outwash aggradation, resulting in a 16 605 m^3 (±39%) volume increase.

5 | RECONSTRUCTION OF THE SPATIAL AND TEMPORAL CHANGES AT THE FJALLSJÖKULL-HRÚTÁRJÖKULL OVERDEEPENINGS

Based upon the observations, quantification and interpretations outlined above, we now present reconstructions of the events in the two depositional overdeepenings (Figures 19 and 20). These reconstructions constitute glacial process-form models that are invaluable because they are based upon events captured in historical imagery and ongoing annual field surveys, which both validate and expand upon similar research programmes initiated in southern Iceland in the 1960s (Howarth, 1971; Price, 1969, 1971, 1980; Welch & Howarth, 1968).

The outwash head that fronts the south Fjallsjökull local overdeepening (case study area 1) was created by the development of ice-marginal drainage around the front of, and over, a shallowing ice lobe in the early 1990s, as evidenced by the pattern of relict drainage channels on the fan surface (Figures 7a and 20a). The origin of the fan's steep and pitted proximal slope, topped by a minor push moraine, is coeval with the later (1994–1998) construction of the thrust moraine in the ice-cored outwash overlying the overdeepening. The switch of marginal meltwater drainage from the kame terrace to a tunnel through the outer thrust block to the fan is recorded by the highest-elevation esker on the west side of the overdeepening (Figure 9). As the thrust blocks and debris-covered ice in the overdeepening melted out and downwasted and the resulting supraglacial lake level fell in response to spillway incision in 2003–2004 (Figure 6), the complex array of eskers was produced. The arcuate, inset series of altitudinally decreasing eskers relate to tunnels draining through the ice and increasingly directed across the overdeepening towards the spillway. The englacial/subglacial engorged eskers were fed by meltwater flowing between the downwasting thrust block margins and the proximal fan slope and then re-entering the ice, partially directed by fractures but also driven by the hydraulic gradient towards the spillway. The highly fractured stagnant ice that remained on the north part of the overdeepening floor as late as 2016 was tunnelled and its fractures infilled by the runoff in the Hrútá (Figures 9i and 12).

The south Fjallsjökull local overdeepening constitutes an excellent example of typical Icelandic outwash head development formed by the combination of ice-marginal drainage and fan construction around a downwasting snout and the thrusting of stagnant ice against the fans' proximal slope. This creates a fan of asymmetrical long profile with a pitted to hummocky adverse slope and forming a depositional overdeepening (Figure 20a). The glacial hydrology of this overdeepening, as recorded by the esker complex, was characterized by englacial drainage tunnels whose migration downwards through the ice was concomitant with a switch in drainage direction from the fan apex in the southwest to the downcutting spillway in the east. All of the large eskers in case study area 1 document the bypassing of the overdeepening by englacial meltwater tunnels grading to outlet

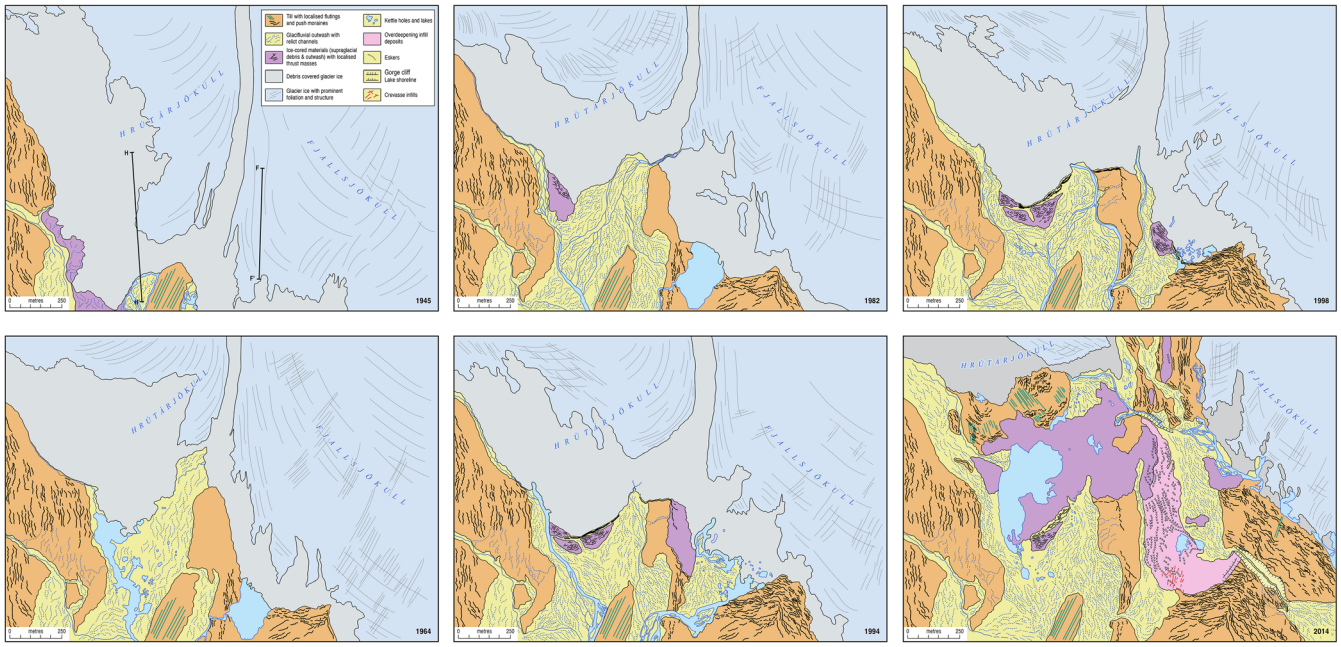

FIGURE 19 Palaeogeographic reconstructions of glacier change and landform development for the Fjallsjökull-Hrútárjökull foreland based on aerial imagery for 1945, 1964, 1982, 1994, 1998 and 2011. Profiles H–H′ and F–F′ on the 1945 map demarcate the positions of the transects in Figure 20.

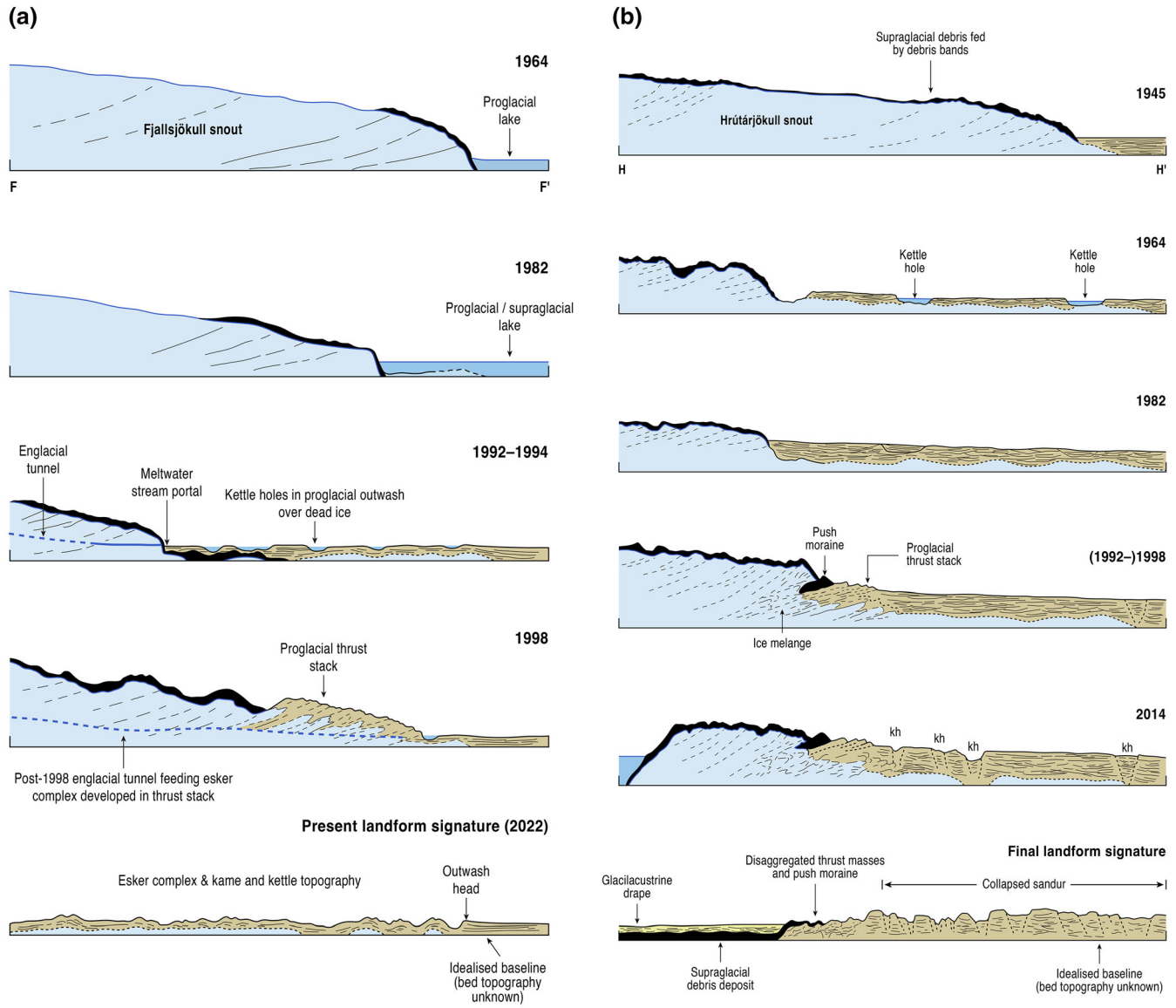

FIGURE 20 Conceptual models of outwash head/depositional overdeepening development and their associated landform–sediment associations for Fjallsjökull (a) and Hrútárjökull (b). Locations of transects are demarcated in Figure 19. See text for details.

portals at higher elevations than the overdeepening floor, compatible with observations and proposals forwarded by Spedding & Evans (2002), Swift et al. (2006) and Bennett & Evans (2012) that most meltwater bypasses the Icelandic south coast overdeepenings, at least during snout downwasting. Englacial esker production here also further verifies process-form models compiled by Price (1965, 1966, 1969) and Howarth (1971) and developed by Gustavson and Boothroyd (1987), Evans and Twigg (2002) and Storrar et al. (2015, 2020).

The recent emergence of the Hrútárjökull depositional overdeepening (case study areas 2, 3 and 4) has occurred through the production of the large lake as a result of rapid melting of the extensive area of debris-covered snout on the south margin of Hrútárjökull (Figures 7b, 19 and 20b). This part of the snout was driven forward during the 1990s, forming a minor push moraine fronted by thrust blocks of ice-cored outwash. The thrust blocks are part of an area of coalescent sandur fans that prograded from the southwest margin of Hrútárjökull and the re-entrant that was created by the coalescence of the Hrútárjökull and Fjallsjökull lobes. This formed a northward-expanding linear sandur in front of the receding ice margins from the late 1930s until around 1998; an ice-dammed lake (Ærfjallslón), located in a valley on the north margin of Hrútárjökull (Figure 2), decanted jökulhlaups onto this sandur via the suture zone of the two glaciers until the mid-20th century (Gudmundsson et al., 2019). The collapse and pitting of the thrust blocks is contiguous with similar, large-scale disturbance in non-thrust sandur in case study area 3, where the most expansive collapse features started in 1992 as minor pitting over the area of what was debris-covered ice in 1945 (Figure 20b). This evolved into extensively pitted and partially glacifluvially buried terrain in 1954. By around 1964, an extensive lake joined up the pits, with drainage flowing from the southwest margin of Hrútárjökull, essentially representing the underlying precursor overdeepening (Figures 19 and 20b). This ice was repeatedly covered by aggrading outwash from the southwest margin of Hrútárjökull in 1988–1994 and from the re-entrant between Hrútárjökull and Fjallsjökull (to the north) in 1968 and 1980–1982, finally being terraced in 1998 when large pits also appeared. Hence, from 2014 to 2022, the large-scale collapse observed in case study area 3 and extending around the eastern edge of the former 1998 readvance

margin demarcates the extent of buried glacier from around 1945, constituting an example of snout burial by prograding sandar.

The circumstances dictating extensive ice burial after 1945 are entirely the same as those for the development of the lake in case study area 2 after 1998; this part of the foreland is occupied through time by substantial amounts of debris-covered ice on the right lateral side of Hrútárjökull, so that any phase of incremental stagnation (sensu Bennett & Evans, 2012; Eyles, 1983) following increased pulses of supraglacial debris will result in the accumulation of proglacial outwash around areas of persistent and slowly downwasting snout, whose ablation rate is significantly retarded compared to the rest of the glacier margin. The downwasting debris-covered part of the Hrútárjökull snout is clearly visible in 1945 aerial imagery and begins collapsing and forming large lakes in 1954 and 1964, but this is curtailed by outwash progradation beginning in 1968 (Figures 2 and 7b). This prograding outwash buries not only the remaining glacier ice but also the older outwash head, which presumably lies beneath the post-1968 outwash head (Figures 19 and 20b). This superimposition of outwash heads and buried ice helps to explain the abnormally large area and depth of sandur collapse due to ice melt-out on the Hrútárjökull foreland.

6 | DISCUSSION

The glacial landsystem signature of the Fjallsjökull-Hrútárjökull foreland as compiled by Chandler, Chandler, et al. (2020) reflects that of active temperate piedmont lobes consistent with those previously reported from southern Iceland (e.g. Bennett et al., 2010; Evans & Orton, 2015; Evans & Twigg, 2002; Evans et al., 2009, 2016, 2017a, 2018; Evans, Ewertowski, et al., 2019; Price, 1969). However, ongoing rapid glacier change, as outlined above, has facilitated both an appreciation of developments of azonal and intrazonal land facets related to localized glacier–terrain interactions as well as the opportunity to quantify glacial landform development and temporal change more generally. Specifically, this entails the genesis of complex glacifluvial sediment–landform associations, in places associated with the hummocky terrain of incremental stagnation, for which previous modern analogue, real-time survey examples are globally relatively few in number (e.g. Bennett & Evans, 2012; Evans et al., 2022; Ewertowski, Tomczyk, et al., 2019; Eyles, 1979, 1983; Gustavson & Boothroyd, 1987; Howarth, 1971; Kjær & Krüger, 2001; Price, 1965, 1966, 1969, 1971, 1980; Storrar et al., 2015; Welch & Howarth, 1968). The combination of repeat aerial imagery, glacier snout oscillation records and field observations at Fjallsjökull-Hrútárjökull facilitates the reconstruction of two interlinked glacial process-form regimes, relating to outwash heads and depositional overdeepenings, which constitute azonal signatures in the active temperate glacial landsystem (Figures 19 and 20).

Of particular significance are the evolutionary stages of outwash head development, which occur through the progradation and aggradation of glacifluvial outwash deposits (sandur) around masses of debris-rich/debris-covered glacier snout. The occurrence of such slowly ablating parts of glacier margins appears crucial to the development of these sandar and the burying of unusually large ice masses, similar to those recorded for example at the Breiðamerkurjökull supraglacial fan sites (Price, 1969; Storrar et al., 2015, 2020); in both settings the emergence of englacial eskers is diagnostic of buried snout ice. Phases of extensive burial of glacier ice by outwash, similar to that observed at Hrútárjökull, are more likely to occur where debris-covered ice becomes isolated from the receding snout (incremental stagnation; Bennett & Evans, 2012; Eyles, 1979). In the case of repeat events this can result in superimposition of outwash heads (Figures 19 and 20) or features such as dead-ice sinks and moats as proposed by Fleisher (1986).

The collapse of the sandur overlying the former 1945 Hrútárjökull ice margin and the emergence of the outwash head has been delayed by the post-1945 burial of the remnant buried glacier ice. The rapid collapse of the overlying sandur reflects large-scale ice melt-out at depth since the end of the 20th century. The 1990s readvance resulted in the delivery of another large area of debris-covered snout (later detached from the main body of the glaciers because of the steep bedrock step) into the ice-cored terrain of the post-1945 outwash head. This thereby constituted the partial superimposition of snout ice of two separate phases of incremental stagnation; the ice mélange visible in the outermost exposure of the 1990s readvance snout (Figure 15) likely represents the thrusting and entrainment of older buried glacier ice, especially as it extends beneath the ice-cored thrust blocks of outwash. Several eskers were also visible within the debris-covered snout in 2014 (Figure 4); however, in contrast to Fjallsjökull overdeepening, they were quickly destroyed as the buried ice downwasted.

The south Fjallsjökull outwash head and depositional overdeepening is less complicated in that it records outwash progradation around the thrust blocks created by the 1990s readvance into ice-cored outwash deposits. The southerly shallowing erosional basin within the outwash-cored Fitjaöldur ridge was occupied by a relatively stable supraglacial and then proglacial lake from 1954 until around 1992, after which it had infilled with an outwash fan. Supraglacial outwash accumulating along the receding glacier margin from 1992 to 1994 was then pushed into the fan as a proglacial thrust mass during the 1990s readvance, creating the pitted and esker-fed outwash head on the north side of the re-occupied fan surface. Preserved after ice core melt-out in this scenario are the englacial esker networks indicative of an evolving glacier hydrology controlled by marginal fan and lake outlet evolution. The ice-marginal/engorged nature of these eskers is diagnostic of meltwater pathways and glacifluvial/inwash processes operating along lateral margins of temperate glaciers, linking partially collapsed kame terrace, esker and minor push moraines, all containing significant water-worked debris, in a complex landform–sediment assemblage that is often oversimplified in glacial landform classifications as kame and kettle topography.

The uncovering of overdeepenings in Iceland has been an important development in the recognition of azonal landsystem signatures, especially those fronted by outwash heads and hence at least partially depositional in origin. This is a prime example of local topographic conditions temporarily switching the predominant process-form regime during overall ice recession and is being observed at an increasing number of Iceland glacier snouts (e.g. Bennett & Evans, 2012; Evans & Orton, 2015; Phillips et al., 2013). The creation of depositional overdeepenings involves the build-up of proglacial, ice-contact outwash fans or outwash heads as a glacier snout progressively overrides its own sandur (e.g. Evans, Ewertowski, et al., 2019;

Thompson & Jones, 1986). During snout recession from the steeper proximal, ice-contact slope of the fan, proglacial meltwater drainage becomes confined between the ice front and the outwash head, resulting in the partial burying of the downwasting snout with glacifluvial sediment in the form of inset kame terraces, eskers and pitted outwash, all of which are prone to bulldozing and push-moraine formation or even thrust-block construction. What emerges is a fan with an asymmetrical cross profile, comprising a steep, hummocky and locally terraced proximal slope and a shallow, distal and undisturbed sandur surface (e.g. Evans & Orton, 2015; Figures 19 and 20).

Although pressurized subglacial drainage pathways entering the overdeepening from up-glacier may be forced to rise the adverse slope and thereby supercool (e.g. Larson et al., 2010; Roberts et al., 2002), englacial tunnels producing eskers in downwasting glaciers have been seen to operate at a level within the snout that is controlled by the relatively higher base level created by fan aggradation (e.g. englacial eskers emerging at Kviarjokull; Bennett & Evans, 2012; Phillips et al., 2017; Spedding & Evans, 2002). As emergence fountains are regularly observed around and on south Icelandic glacier snouts (e.g. Tweed et al., 2018), it is clear that subglacial meltwater is also rising through the snout ice to the higher levels of ice-marginal outwash fans and indeed may prograde fans over shallow snouts if the emergence occurs some distance up-snout (Gustavson & Boothroyd, 1987; Price, 1969). Additionally, the process of inwash from lateral meltwater steams and/or englacial tunnels, observed in both of the Fjallsjökull-Hrútárjökull overdeepenings, can result in more extensive burying of the snout, giving rise to collapsing fan surfaces and emerging eskers during later melt-out behind the outwash head (Evans & Twigg, 2002; Price, 1969; Storrar et al., 2015; Figures 19 and 20).

The process of inwash burying a shallowing snout was captured by Price (1971) when an ice-dammed lake along the west margin of Breiðamerkurjökull catastrophically drained and buried the glacier snout under an outwash fan. Parts of the fan collapsed by up to 4 m due to the melt-out of buried glacier ice over a period of 4 years, with expansion of pits into interconnected lakes taking place after a further 5 years; the fan apex in 2018 appeared as hummocky terrain. The emergence of eskers through such collapsing fan surfaces, as demonstrated by repeat surveys of the Breiðamerkurjökull snout and foreland (Evans & Twigg, 2002; Price, 1969; Storrar et al., 2015), reveals not only the existence of englacial to subglacial drainage networks beneath outwash fans but also documents the supraglacial nature rather than jökulhlaup origins of extensively pitted or hummocky outwash often classified as kame and kettle topography.

All of these circumstances result in eskers grading to fan apexes (e.g. Bennett & Evans, 2012; Price, 1969; Storrar et al., 2015) but the operation of tunnels feeding proglacial fans becomes more difficult once snout downwasting has resulted in the ice surface falling below the fan apex, thereby lowering the base level of the glaciohydraulic system below the immediate surrounding topography. What has been observed in such situations is the formation of ice-margin parallel esker formation along the outwash head cliff in tunnels draining towards the nearest area of lower topography (Boulton, 1986; Storrar et al., 2015, 2020). In situations where meltwater cannot drain effectively from behind the outwash head to lower topography, proglacial lakes will form (Bennett & Evans, 2012; Bennett et al., 2010; Evans, Ewertowski, et al., 2019; Figures 19 and 20), giving rise to the draping of glacilacustrine sediments over, and inter-connecting with, ice-contact glacifluvial assemblages and buried glacier ice.

The recent amount and rate of buried ice loss by melt-out on the south Fjallsjökull-Hrútárjökull foreland, as calculated using DoDs (Table 2; Figure 13) for the period 2014–2022, varies significantly. For context, the average cumulative elevation loss at the debris-covered snout of Hrútárjökull between 2016 and 2022 was 4.5 m. Similarly, the cumulative volume change in the period 2016–2022 was −600 000 m^3. This is reflective of glacier surface change in the present climate warming scenario. Compared to this, buried ice loss ranges from very low totals and rates in the Fjallsjökull overdeepening, related to the adverse slope and the esker network, up to the highest rate relating to the removal of the Hrútárjökull debris-covered snout from its overdeepening. The latter has been subject to the greatest amount of volume change, increasing from ∼500 000 m^3 in the 2014/2015 melt season to ∼1 600 000 m^3 by the 2018/2019 melt season, after which the dynamics of volume change have been greatly reduced. The buried glacier ice around the southern edge of this overdeepening (collapsed sandur) has melted out at a much slower rate (cumulative volume loss increasing from ∼100 000 m^3 in 2015/2016 to ∼300 000 m^3 in 2022), but has nevertheless gradually exposed the former outwash head, with an average rate of buried ice loss of ∼21 000 m^3 per year over the last 3 years. This quantity and rate of buried ice melting is reflected also in the hummocky terrain/medial moraine area on the Fitjaöldur remnant. Also related to buried ice melt-out is the volume change of the 1990s thrust moraine, within which volume loss has increased at a similar rate, but with smaller totals, from ∼50 000 m^3 in 2015/2016 to ∼120 000 m^3 in 2022.

In contrast to the large volumes of buried ice loss over the Hrútárjökull overdeepening, landscape change has been more modest and volume change has stabilized in the esker network and adverse slope of the Fjallsjökull overdeepening since around 2016/2017. This no doubt reflects the significantly greater supraglacial debris cover and glacifluvial snout burial that has characterized the Hrútárjökull snout since 1945, which has retarded ablation and thereby delayed glacier ice melt. The higher rates of volume change on the inner part of the Fjallsjökull overdeepening since 2014 relate to the later date of ice recession from this area, amounting to buried ice removal at similar rates to those in the Hrútárjökull collapsed sandur and hummocky terrain/medial moraine, the latter being partly related to supraglacial melting of Fjallsjökull at its suture point with Hrútárjökull.

Each of the individual study area rates and totals for volume change reported here reflect the variability in paraglacial landscape response to deglaciation (cf. Ballantyne, 2002; Ballantyne & Benn, 1994; Bennett & Evans, 2012; Schomacker & Kjaer, 2007, 2008), wherein the debris-charged snout of Hrútárjökull has resulted in the retarded ablation that drives incremental stagnation (sensu Bennett & Evans, 2012; Eyles, 1983). This was exacerbated by the extensive burial of the downwasting Hrútárjökull snout by the sandur fan that emanated from the suture zone between the glacier snouts when they were coalescent. The large volume of outwash in this sandur was at least partially due to jökulhlaup drainage from the Ærfjallslón ice-dammed lake between the late 1930s until the mid-20th century (Gudmundsson et al., 2019). Glacier snout loss was further interrupted by the mid-1990s readvance, during which buried ice, supraglacial debris and ice-cored outwash was proglacially thrust-stacked.

Consequently, complete de-icing of the Hrútárjökull snout in response to post-1945 warming was delayed until around 2014, resulting in significant landscape change over a period of 8 years (average elevation loss between 2014 and 2022 was 6.3 m, or 0.8 m a^{-1}).

7 | CONCLUSION

The development of localized landform–sediment assemblages that contrast with the overall landsystem signature of an active temperate glacier foreland is azonal or even intrazonal in nature, and they typically include the products of overdeepenings and intermittent readvances. The recent rapid recession of such glaciers has provided important information on the development of meltwater drainage characteristics in relation to overdeepenings, in particular. Our analysis of the historical and ongoing developments (1945–2022) of the landform–sediment associations of two depositional overdeepenings on the Fjallsjökull-Hrútárjökull foreland provide invaluable ingredients for the compilation of glacial process-form models for the origins of outwash heads, kame and kettle topography and englacial esker networks. The importance of inwash from lateral meltwater streams and/or englacial tunnels, as well as proglacial outwash in the burial of large areas of debris-covered, downwasting glacier snouts in the production of extensive sandur collapse, is also recorded in these models; the Fjallsjökull-Hrútárjökull case study demonstrates that such depositional contexts are inextricably linked to incremental stagnation. Moreover, there is clear evidence inherent within these models that drainage tunnel and esker development in particular is taking place englacially rather than subglacially, so that large volumes of meltwater drainage appear to be bypassing the deepest parts of depositional overdeepenings during advanced stages of glacier downwasting. This accumulation of significant volumes of glacifluvial sediment within and over glacier snouts, actively downwasting into depositional overdeepenings, is producing an outwash head landsystem signature that is diagnostic of active temperate glacier response to rapid climate change.

ACKNOWLEDGEMENTS

Scientific research permits allowing fieldwork at Fjallsjökull-Hrútárjökull over a number of years were provided by Regína Hreinsdóttir, Helga Árnadóttir and Steinnun Hödd Harðardóttir on behalf of the Vatnajökull National Park. Research declarations were also provided by RANNÍS (The Icelandic Centre for Research) for overseas research in Iceland. This paper includes research that was funded by the National Science Centre, Poland (Narodowe Centrum Nauki; Grant No. 2019/35/B/ST10/03928).

CONFLICT OF INTEREST STATEMENT

The authors have no conflict of interest.

DATA AVAILABILITY STATEMENT

All data will be made accessible by the authors upon reasonable request.

ORCID

David J. A. Evans https://orcid.org/0000-0002-1840-2513

Benjamin M. P. Chandler https://orcid.org/0000-0003-1532-9696

REFERENCES

Ballantyne, C.K. (2002) Paraglacial geomorphology. *Quaternary Science Reviews*, 21, 1935–2017. Available from: https://doi.org/10.1016/S0277-3791(02)00005-7

Ballantyne, C.K. & Benn, D.I. (1994) Paraglacial slope adjustment and resedimentation following recent glacier retreat, Fåbergstølsdalen, Norway. *Arctic and Alpine Research*, 26, 255–69.

Benn, D.I. & Evans, D.J.A. (2010) *Glaciers and Glaciation*. London: Hodder.

Benn, D.I., Kirkbride, M.P., Owen, L.A. & Brazier, V. (2003) Glaciated valley landsystems. In: Gooster, L. & Evans, D. (Eds.) *Glacial Landsystems*. London: Arnold, pp. 372–406.

Bennett, G.L. & Evans, D.J.A. (2012) Glacier retreat and landform production on an overdeepened glacier foreland: The debris-charged glacial landsystem at Kviarjokull, Iceland. *Earth Surface Processes and Landforms*, 37(15), 1584–1602. Available from: https://doi.org/10.1002/esp.3259

Bennett, G.L., Evans, D.J.A., Carbonneau, P. & Twigg, D.R. (2010) Evolution of a debris-charged glacier landsystem, Kviárjökull, Iceland. *Journal of Maps*, 6(1), 40–67. Available from: https://doi.org/10.4113/jom.2010.1114

Björnsson, H., Pálsson, F., Sigurðsson, O. & Flowers, G.E. (2003) Surges of glaciers in Iceland. *Annals of Glaciology*, 36, 82–90. Available from: https://doi.org/10.3189/172756403781816365

Boulton, G.S. (1986) Push-moraines and glacier-contact fans in marine and terrestrial environments. *Sedimentology*, 33(5), 677–698. Available from: https://doi.org/10.1111/j.1365-3091.1986.tb01969.x

Bradwell, T., Sigurdsson, O. & Everest, J. (2013) Recent, very rapid retreat of a temperate glacier in SE Iceland. *Boreas*, 42(4), 959–973. Available from: https://doi.org/10.1111/bor.12014

Chandler, B.M.P., Chandler, S.J.P., Evans, D.J.A., Ewertowski, M.W., Lovell, H., Roberts, D.H. et al. (2020) Sub-annual moraine formation at an active temperate Icelandic glacier. *Earth Surface Processes and Landforms*, 45(7), 1622–1643. Available from: https://doi.org/10.1002/esp.4835

Chandler, B.M.P., Evans, D.J.A., Chandler, S.J.P., Ewertowski, M.W., Lovell, H., Roberts, D.H. et al. (2020) The glacial landsystem of Fjallsjökull, Iceland: Spatial and temporal evolution of process-form regimes at an active temperate glacier. *Geomorphology*, 361, 107192. Available from: https://doi.org/10.1016/j.geomorph.2020.107192

Chandler, B.M.P., Evans, D.J.A. & Roberts, D.H. (2016a) Characteristics of recessional moraines at a temperate glacier in SE Iceland: Insights into patterns, rates and drivers of glacier retreat. *Quaternary Science Reviews*, 135, 171–205. Available from: https://doi.org/10.1016/j.quascirev.2016.01.025

Chandler, B.M.P., Evans, D.J.A. & Roberts, D.H. (2016b) Recent retreat at a temperate Icelandic glacier in the context of the last ~80 years of climate change in the North Atlantic region. *Arktos*, 2(1), 24. Available from: https://doi.org/10.1007/s41063-016-0024-1

Chandler, B.M.P., Evans, D.J.A., Roberts, D.H., Ewertowski, M. & Clayton, A.I. (2016) Glacial geomorphology of the Skálafellsjökull foreland, Iceland: A case study of 'annual' moraines. *Journal of Maps*, 12, 905–916.

Chandler, B.M.P., Lovell, H., Boston, C.M., Lukas, S., Barr, I.D., Benediktsson, Í.Ö. et al. (2018) Glacial geomorphological mapping: A review of approaches and frameworks for best practice. *Earth-Science Reviews*, 185, 806–846. Available from: https://doi.org/10.1016/j.earscirev.2018.07.015

Cook, K.L. & Dietze, M. (2019) Short communication: A simple workflow for robust low-cost UAV-derived change detection without ground control points. *Earth Surface Dynamics*, 7(4), 1009–1017. Available from: https://doi.org/10.5194/esurf-7-1009-2019

de Haas, T., Nijland, W., McArdell, B.W. & Kalthof, M.W.M.L. (2021) Case report: Optimization of topographic change detection with UAV structure-from-motion photogrammetry through survey co-alignment. *Frontiers in Remote Sensing*, 2, 626810. Available from: https://doi.org/10.3389/frsen.2021.626810

Dell, R., Carr, R., Phillips, E. & Russell, A.J. (2019) Response of glacier flow and structure to proglacial lake development and climate at

Fjallsjökull, South-East Iceland. *Journal of Glaciology*, 65(250), 321–336. Available from: https://doi.org/10.1017/jog.2019.18

Evans, D.J.A. (2003) *Glacial Landsystems*. London: Arnold.

Evans, D.J.A. (2005) The glacier-marginal landsystems of Iceland. In: Caseldine, C.J., Russell, A.J., Hardardottir, J. & Knudsen, O. (Eds.) *Iceland: Modern Processes and Past Environments*. Amsterdam: Elsevier, pp. 93–126.

Evans, D.J.A. (2009) Glacial geomorphology at Glasgow. *Scottish Geographical Journal*, 125(3–4), 285–320. Available from: https://doi.org/10.1080/14702540903364310

Evans, D.J.A. (2013) The glacial and periglacial research – geomorphology and retreating glaciers. In: Shroder, J. (Ed. in Chief), Giardino, R. & Harbor, J. (Eds.) *Glacial and Periglacial Geomorphology*, Treatise on Geomorphology, vol. 8. Academic Press: San Diego, CA, pp. 460–478.

Evans, D.J.A. & Hiemstra, J.F. (2005) Till deposition by glacier submarginal, incremental thickening. *Earth Surface Processes and Landforms*, 30(13), 1633–1662. Available from: https://doi.org/10.1002/esp.1224

Evans, D.J.A. & Orton, C. (2015) Heinabergsjökull and Skalafellsjökull, Iceland: Active temperate piedmont lobe and outwash head glacial landsystem. *Journal of Maps*, 11(3), 415–431. Available from: https://doi.org/10.1080/17445647.2014.919617

Evans, D.J.A. & Twigg, D.R. (2002) The active temperate glacial landsystem: A model based on Breiðamerkurjökull and Fjallsjökull, Iceland. *Quaternary Science Reviews*, 21(20–22), 2143–2177. Available from: https://doi.org/10.1016/S0277-3791(02)00019-7

Evans, D.J.A., Ewertowski, M. & Orton, C. (2016) Fláajökull (north lobe), Iceland: Active temperate piedmont lobe glacial landsystem. *Journal of Maps*, 12(5), 777–789. Available from: https://doi.org/10.1080/17445647.2015.1073185

Evans, D.J.A., Ewertowski, M. & Orton, C. (2017a) Skaftafellsjökull, Iceland: Glacial geomorphology recording glacier recession since the Little Ice Age. *Journal of Maps*, 13(2), 358–368. Available from: https://doi.org/10.1080/17445647.2017.1310676

Evans, D.J.A., Ewertowski, M. & Orton, C. (2017b) The glaciated valley landsystem of Morsárjökull, Southeast Iceland. *Journal of Maps*, 13(2), 909–920. Available from: https://doi.org/10.1080/17445647.2017.1401491

Evans, D.J.A., Ewertowski, M., Orton, C. & Graham, D.J. (2018) The glacial geomorphology of the ice cap piedmont lobe landsystem of East Myrdalsjokull, Iceland. *Geosciences*, 8(6), 194. Available from: https://doi.org/10.3390/geosciences8060194

Evans, D.J.A., Ewertowski, M., Roberts, D.H. & Tomczyk, A.M. (2022) The historical emergence of a geometric and sinuous ridge network at the Hørbyebreen polythermal glacier snout, Svalbard and its use in the interpretation of ancient glacial landforms. *Geomorphology*, 406, 108213. Available from: https://doi.org/10.1016/j.geomorph.2022.108213

Evans, D.J.A., Ewertowski, M.W. & Orton, C. (2019) The glacial landsystem of Hoffellsjökull, SE Iceland: Contrasting geomorphological signatures of active temperate glacier recession driven by ice lobe and bed morphology. *Geografiska Annaler*, 101A, 249–276.

Evans, D.J.A., Guðmundsson, S., Vautrey, J.L., Fearnyough, K. & Southworth, W.G. (2019) Testing lichenometric techniques in the production of a new growth-rate (curve) for the Breiðamerkurjökull foreland, Iceland, and the analysis of potential climatic drivers of glacier recession. *Geografiska Annaler*, 101A, 225–248.

Evans, D.J.A., Lemmen, D.S. & Rea, B.R. (1999) Glacial landsystems of the southwest Laurentide Ice Sheet: modern Icelandic analogues. *Journal of Quaternary Science*, 14(7), 673–691. Available from: https://doi.org/10.1002/(SICI)1099-1417(199912)14:7<673::AID-JQS467>3.0.CO;2-#

Evans, D.J.A., Shand, M. & Petrie, G. (2009) Maps of the snout and proglacial landforms of Fjallsjökull, Iceland (1945, 1965, 1998). *Scottish Geographical Journal*, 125, 304–312.

Ewertowski, M.W., Evans, D.J.A., Roberts, D.H., Tomczyk, A.M., Ewertowski, W. & Pleksot, K. (2019) Quantification of historical landscape change on the foreland of a receding polythermal glacier, Hørbyebreen, Svalbard. *Geomorphology*, 325, 40–54. Available from: https://doi.org/10.1016/j.geomorph.2018.09.027

Ewertowski, M.W., Tomczyk, A.M., Evans, D.J.A., Roberts, D.H. & Ewertowski, W. (2019) Operational framework for rapid, very-high resolution mapping of glacial geomorphology using low-cost unmanned aerial vehicles and structure-from-motion approach. *Remote Sensing*, 11(1), 65. Available from: https://doi.org/10.3390/rs11010065

Eyles, N. (1979) Facies of supraglacial sedimentation on Icelandic and alpine temperate glaciers. *Canadian Journal of Earth Sciences*, 16(7), 1341–1361. Available from: https://doi.org/10.1139/e79-121

Eyles, N. (1983) Modern Icelandic glaciers as depositional models for "hummocky moraine" in the Scottish highlands. In: Evenson, E.B., Schluchter, C. & Rabassa, J. (Eds.) *Tills and Related Deposits*. Rotterdam: Balkema, pp. 47–59.

Fleisher, P.J. (1986) Dead ice sinks and moats: Environments of stagnant ice deposition. *Geology*, 14(1), 39–42. Available from: https://doi.org/10.1130/0091-7613(1986)14<39:DSAMEO>2.0.CO;2

Guðmundsson, S., Björnsson, H., Pálsson, F., Magnússon, E., Sæmundsson, Þ. & Jóhannesson, T. (2019) Terminus lakes on the south side of Vatnajökull ice cap SE-Iceland. *Jökull*, 69, 1–34.

Guðmundsson, S. & Evans, D.J.A. (2022) Geomorphological map of Breiðamerkursandur 2018: The historical evolution of an active temperate glacier foreland. *Geografiska Annaler*, 104(4), 298–332. Available from: https://doi.org/10.1080/04353676.2022.2148083

Gustavson, T.C. & Boothroyd, J.C. (1987) A depositional model for outwash, sediment sources and hydrologic characteristics, Malaspina Glacier, Alaska: a modern analog of the southeastern margin of the Laurentide Ice Sheet. *Geological Society of America Bulletin*, 99, 187–200. Available from: https://doi.org/10.1130/0016-7606(1987)99<187:ADMFOS>2.0.CO;2

Hannesdóttir, H., Björnsson, H., Pálsson, F., Aðalgeirsdóttir, G. & Guðmundsson, S. (2014) Variations of Southeast Vatnajökull ice cap (Iceland) 1650–1900 and reconstruction of the glacier surface geometry at the Little Ice Age maximum. *Geografiska Annaler*, 97A, 237–264.

Hannesdóttir, H., Björnsson, H., Pálsson, F., Aðalgeirsdóttir, G. & Guðmundsson, S. (2015) Area, volume and mass changes of Southeast Vatnajökull ice cap, Iceland, from the Little Ice Age maximum in the late 19th century to 2010. *The Cryosphere*, 9(2), 565–585. Available from: https://doi.org/10.5194/tc-9-565-2015

Howarth, P.J. (1971) Investigations of two eskers at eastern Breiðamerkurjökull, Iceland. *Arctic and Alpine Research*, 3, 305–318.

Hugenholtz, C.H., Whitehead, K., Brown, O.W., Barchyn, T.E., Moorman, B.J., LeClair, A. et al. (2013) Geomorphological mapping with a small unmanned aircraft system (sUAS): Feature detection and accuracy assessment of a photogrammetrically-derived digital terrain model. *Geomorphology*, 194, 16–24. Available from: https://doi.org/10.1016/j.geomorph.2013.03.023

Kirkbride, M.P. (2000) Ice marginal geomorphology and Holocene expansion of debris-covered Tasman Glacier, New Zealand. In: Nakawo, M., Raymond, C. & Fountain, A. (Eds.) *Debris-covered Glaciers*, Vol. 264. IAHS Publication, pp. 211–217.

Kjær, K.H. & Krüger, J. (2001) The final phase of dead ice moraine development: processes and sediment architecture, Kotlujokull, Iceland. *Sedimentology*, 48, 935–952. Available from: https://doi.org/10.1046/j.1365-3091.2001.00402.x

Krüger, J. (1994) Glacial processes, sediments, landforms, and stratigraphy in the terminus region of Myrdalsjökull, Iceland. *Folia Geographica Danica*, 21, 1–233.

Larson, G.J., Lawson, D.E., Evenson, E.B., Knudsen, O., Alley, R.B. & Phanikumar, M.S. (2010) Origin of stratified basal ice in outlet glaciers of Vatnajokull and Oraefajokull, Iceland. *Boreas*, 39, 457–470. Available from: https://doi.org/10.1111/j.1502-3885.2009.00134.x

Magnusson, E., Palsson, F., Bjornsson, H. & Gudmundsson, S. (2012) Removing the ice cap of Oraefajokull central volcano, SE Iceland:

mapping and interpretation of bedrock topography, ice volumes, subglacial troughs and implications for hazard assessment. *Jokull*, 62, 132–150.

Maizels, J.K. (1997) Jokulhlaup deposits in proglacial areas. *Quaternary Science Reviews*, 16(7), 793–819. Available from: https://doi.org/10.1016/S0277-3791(97)00023-1

Mannerfelt, C.M. (1945) Nagra glacialmorfologiska formelement. *Geografiska Annaler*, 27, 1–239.

Mannerfelt, C.M. (1949) Marginal drainage channels as indicators of the gradients of quaternary ice caps. *Geografiska Annaler*, 31, 194–199.

Midgley, N.G., Tonkin, T.N., Graham, D.J. & Cook, S.J. (2018) Evolution of high-Arctic glacial landforms during deglaciation. *Geomorphology*, 311, 63–75. Available from: https://doi.org/10.1016/j.geomorph.2018.03.027

Phillips, E.R., Everest, J., Evans, D.J.A., Finlayson, A., Ewertowski, M., Guild, A. et al. (2017) Concentrated, pulsed axial flow: structural glaciological evidence from Kviarjokull in SE Iceland. *Earth Surface Processes and Landforms*, 42, 1901–1922. Available from: https://doi.org/10.1002/esp.4145

Phillips, E.R., Finlayson, A. & Jones, L. (2013) Fracturing, block-faulting and moulin development associated with progressive collapse and retreat of a polar maritime glacier: Virkisjökull-Falljökull, SE Iceland. *Journal of Geophysical Research, Earth Surface*, 118, 1–17.

Price, R.J. (1965) The changing proglacial environment of the Casement Glacier, Glacier Bay, Alaska. *Transactions of the Institute of British Geographers*, 36(36), 107–116. Available from: https://doi.org/10.2307/621457

Price, R.J. (1969) Moraines, sandar, kames and eskers near Breiðamerkurjökull, Iceland. *Transactions of the Institute of British Geographers*, 46, 17–43.

Price, R.J. (1966) Eskers near the Casement Glacier, Alaska. *Geografiska Annaler*, 48(3), 111–125. Available from: https://doi.org/10.1080/04353676.1966.11879733

Price, R.J. (1971) The development and destruction of a sandur, Breiðamerkurjökull, Iceland. *Arctic and Alpine Research*, 3(3), 225–237. Available from: https://doi.org/10.2307/1550195

Price, R.J. (1973) *Glacial and Fluvioglacial Landforms*. London: Longmans.

Price, R.J. (1980) Rates of geomorphological changes in proglacial areas. In: Cullingford, R.A., Davidson, D.A. & Lewin, J. (Eds.) *Timescales in Geomorphology*. Chichester: Wiley, pp. 79–93.

Roberts, M.J., Tweed, F.S., Russell, A.J., Knudsen, O., Lawson, D.E., Larson, G.J. et al. (2002) Glaciohydraulic supercooling in Iceland. *Geology*, 30, 439–442. Available from: https://doi.org/10.1130/0091-7613(2002)030<0439:GSII>2.0.CO;2

Russell, A.J., Knight, P.G. & van Dijk, T.A.G.P. (2001) Glacier surging as a control on the development of proglacial, fluvial landforms and deposits, Skeiðarársandur, Iceland. *Global and Planetary Change*, 28(1–4), 163–174. Available from: https://doi.org/10.1016/S0921-8181(00)00071-0

Russell, A.J., Roberts, M.J., Fay, H., Marren, P.M., Cassidy, N.J., Tweed, F.S. et al. (2006) Icelandic jokulhlaup impacts: implications for ice sheet hydrology, sediment transfer and geomorphology. *Geomorphology*, 75(1-2), 33–64. Available from: https://doi.org/10.1016/j.geomorph.2005.05.018

Schomacker, A. & Kjaer, K.H. (2007) Origin and de-icing of multiple generations of ice-cored moraines at Bruarjokull, Iceland. *Boreas*, 36, 411–425. Available from: https://doi.org/10.1080/03009480701213554

Schomacker, A. & Kjaer, K.H. (2008) Quantification of dead-ice melting in ice-cored moraines at the high arctic glacier Holmstrombreen, Svalbard. *Boreas*, 37, 211–225. Available from: https://doi.org/10.1111/j.1502-3885.2007.00014.x

Schomacker, A., Kruger, J. & Kjaer, K.H. (2009) *The Myrdalsjokull Ice Cap, Iceland: Glacial Processes*. Elsevier, Amsterdam: Sediments and Landforms on an Active Volcano.

Sigurđsson, O., Jónsson, T. & Jóhannesson, T. (2007) Relation between glacier-termini variations and summer temperature in Iceland since 1930. *Annals of Glaciology*, 46, 170–176. Available from: https://doi.org/10.3189/172756407782871611

Śledź, S. & Ewertowski, M.W. (2022) Evaluation of the influence of processing parameters in structure-from-motion software on the quality of digital elevation models and orthomosaics in the context of studies on earth surface dynamics. *Remote Sensing*, 14(6), 1312. Available from: https://doi.org/10.3390/rs14061312

Slomka, J.M. & Eyles, C.H. (2015) Architectural-landsystem analysis of a modern glacial landscape, Solheimajokull, southern Iceland. *Geomorphology*, 230, 75–97. Available from: https://doi.org/10.1016/j.geomorph.2014.11.006

Smith, M.W., Carrivick, J.L. & Quincey, D.J. (2016) Structure from motion photogrammetry in physical geography. *Progress in Physical Geography: Earth and Environment*, 40(2), 247–275. Available from: https://doi.org/10.1177/0309133315615805

Spedding, N. & Evans, D.J.A. (2002) Sediments and landforms at Kvíárjökull, Southeast Iceland: A reappraisal of the glaciated valley landsystem. *Sedimentary Geology*, 149(1–3), 21–42. Available from: https://doi.org/10.1016/S0037-0738(01)00242-1

Storrar, R.D., Evans, D.J.A., Stokes, C.R. & Ewertowski, M. (2015) Controls on the location, morphology and evolution of complex esker systems at decadal timescales, Breiðamerkurjökull, Southeast Iceland. *Earth Surface Processes and Landforms*, 40(11), 1421–1438. Available from: https://doi.org/10.1002/esp.3725

Storrar, R.D., Ewertowski, M., Tomczyk, A.M., Barr, I.D., Livingstone, S.J., Ruffell, A. et al. (2020) Equifinality and preservation potential of complex eskers. *Boreas*, 49(1), 211–231. Available from: https://doi.org/10.1111/bor.12414

Swift, D.A., Evans, D.J.A. & Fallick, A.E. (2006) Transverse englacial debris-rich ice bands at Kviarjokull, southeast Iceland. *Quaternary Science Reviews*, 25, 1708–1718. Available from: https://doi.org/10.1016/j.quascirev.2006.01.003

Thompson, A. & Jones, A. (1986) Rates and causes of proglacial river terrace formation in Southeast Iceland: An application of lichenometric dating techniques. *Boreas*, 15(3), 231–246. Available from: https://doi.org/10.1111/j.1502-3885.1986.tb00928.x

Thórarinsson, S. (1939) Vatnajökull. The scientific results of the Swedish–Icelandic investigations 1936–37–38. Chapter IX. The ice dammed lakes of Iceland with particular reference to their values as indicators of glacier oscillations. *Geografiska Annaler*, 21, 216–242.

Thórarinsson, S. (1943) Vatnajokull. Scientific results of the Swedish–Icelandic investigations 1936–37–38. Chapter XI. *Geografiska Annaler*, 25, 1–54.

Tonkin, T.N., Midgley, N.G., Cook, S.J. & Graham, D.J. (2016) Ice-cored moraine degradation mapped and quantified using an unmanned aerial vehicle: A case study from a polythermal glacier in Svalbard. *Geomorphology*, 258, 1–10. Available from: https://doi.org/10.1016/j.geomorph.2015.12.019

Tweed, F.S., Russell, A.J., Harris, T. & Roberts, M.J. (2018) Supercooled meltwater discharge from Skeidararjokull and Skaftafellsjokull and associated glacial debris entrainment. In: Evans, D.J.A. (Ed.) *Glacial Landsystems of Southeast Iceland: Quaternary Applications - Field Guide*. London: QRA, pp. 50–61.

Waller, R.I., van Dijk, T.A.G.P. & Knudsen, O. (2008) Subglacial bedforms and conditions associated with the 1991 surge of Skeidararjokull, Iceland. *Boreas*, 37(2), 179–194. Available from: https://doi.org/10.1111/j.1502-3885.2007.00017.x

Welch, R. & Howarth, P.J. (1968) Photogrammetric measurements of glacial landforms. *Photogrammetric Record*, 6(31), 75–96. Available from: https://doi.org/10.1111/j.1477-9730.1968.tb00915.x

Westoby, M.J., Brasington, J., Glasser, N.F., Hambrey, M.J. & Reynolds, J.M. (2012) 'Structure-from-motion' photogrammetry: A low-cost, effective tool for geoscience applications. *Geomorphology*, 179, 300–314. Available from: https://doi.org/10.1016/j.geomorph.2012.08.021

Wheaton, J.M., Brasington, J., Darby, S.E., Merz, J., Pasternack, G.B., Sear, D. et al. (2010) Linking geomorphic changes to salmonid habitat at a scale relevant to fish. *River Research Applications*, 26(4), 469–486. Available from: https://doi.org/10.1002/rra.1305

Wheaton, J.M., Brasington, J., Darby, S.E. & Sear, D.A. (2010) Accounting for uncertainty in DEMs from repeat topographic surveys: Improved sediment budgets. *Earth Surface Processes and Landforms*, 35, 136–156.

Whitehead, K., Hugenholtz, C.H., Myshak, S., Brown, O., LeClair, A., Tamminga, A. et al. (2014) Remote sensing of the environment with small unmanned aircraft systems (UASs), part 2: Scientific and commercial applications. *Journal of Unmanned Vehicle Systems*, 02(03), 86–102. Available from: https://doi.org/10.1139/juvs-2014-0007

How to cite this article: Evans, D.J.A., Ewertowski, M.W., Tomczyk, A. & Chandler, B.M.P. (2023) Active temperate glacial landsystem evolution in association with outwash head/depositional overdeepenings. *Earth Surface Processes and Landforms*, 1–26. Available from: https://doi.org/10.1002/esp.5569